



CERN-EP-2023-255
13 November 2023

Measurement of (anti)alpha production in central Pb–Pb collisions at $\sqrt{s_{NN}} = 5.02$ TeV

ALICE Collaboration*

Abstract

In this letter, measurements of (anti)alpha production in central (0–10%) Pb–Pb collisions at a center-of-mass energy per nucleon–nucleon pair of $\sqrt{s_{NN}} = 5.02$ TeV are presented, including the first measurement of an antialpha transverse-momentum spectrum. Owing to its large mass, the production of (anti)alpha is expected to be sensitive to different particle production models. The production yields and transverse-momentum spectra of nuclei are of particular interest because they provide a stringent test of these models. The averaged antialpha and alpha spectrum is compared to the spectra of lighter particles, by including it into a common blast-wave fit capturing the hydrodynamic-like flow of all particles. This fit is indicating that the (anti)alpha also participates in the collective expansion of the medium created in the collision. A blast-wave fit including only protons, (anti)alpha, and other light nuclei results in a similar flow velocity as the fit that includes all particles. A similar flow velocity, but a significantly larger kinetic freeze-out temperature is obtained when only protons and light nuclei are included in the fit. The coalescence parameter B_4 is well described by calculations from a statistical hadronization model but significantly underestimated by calculations assuming nucleus formation via coalescence of nucleons. Similarly, the (anti)alpha-to-proton ratio is well described by the statistical hadronization model. On the other hand, coalescence calculations including approaches with different implementations of the (anti)alpha substructure tend to underestimate the data.

arXiv:2311.11758v2 [nucl-ex] 1 Oct 2024

1 Introduction

During the past five decades the production of light nuclei in heavy-ion reactions has been measured over a broad range of collision energies [1–21]. At center-of-mass energies of up to a few GeV light nucleus production is commonly understood in terms of nuclear break-up where the incoming nuclei disintegrate into lighter nuclear fragments. In contrast to this, the study of the production of antinuclei in heavy-ion collisions is a nascent field that emerged with the availability of heavy-ion colliders [22–38]. In particular, the antialpha was first observed only 13 years ago by the STAR Collaboration in Au–Au collisions at the Relativistic Heavy-Ion Collider (RHIC) [39]. At the Large Hadron Collider (LHC), which provides the highest center-of-mass energies for heavy-ion collisions to date, measurements of the production of nuclei and antinuclei have so far mainly been performed by the ALICE Collaboration in different collision systems [40–57]. Understanding the production mechanism of nuclei and antinuclei in ultrarelativistic collisions could provide deeper insights into the hadronization process and the quantum properties of composite hadronic systems.

Two different approaches exist that describe the production of light (anti)nuclei in heavy-ion collisions. In statistical hadronization models (SHMs), often simply called thermal models, the production of hadrons and nuclei is described in the framework of a grand-canonical ensemble employing only three parameters: temperature T , volume V , and baryo-chemical potential μ_B [58–64]. Previous measurements of the production of light (anti)nuclei in central Pb–Pb collisions¹ by the ALICE Collaboration agreed well with a common SHM fit to all available hadron and nucleus measurements with a temperature of $T = (156.5 \pm 1.5)$ MeV and a baryo-chemical potential of $\mu_B = (0.7 \pm 3.8)$ MeV [62]. The temperature is commonly understood in terms of a chemical freeze-out temperature T_{ch} at which the abundances of hadrons and nuclei are fixed during the evolution of the fireball created in central Pb–Pb collisions [53, 61]. It is compatible with the (pseudo)critical temperature T_c predicted by the lattice QCD calculations for the transition between a hadronic system and a quark–gluon plasma (QGP) at vanishing μ_B [65, 66]. The interpretation in the context of the production of nuclei, however, is not straightforward because significant modifications of the abundances of nuclei are expected from density and cross section arguments due to inelastic processes in the subsequent fireball evolution, often called hadronic phase, below T_{ch} [61, 67, 68]. In another class of models, nucleus formation is conjectured via the coalescence of nucleons in the final state of the system evolution [69–72]. The coalescence process is typically associated with the kinetic freeze-out temperature T_{kin} , which corresponds to the temperature where the inelastic collisions cease and the (transverse) momentum spectra of the particles are frozen [61, 73]. The invariant yield $E_A \frac{d^3 N_A}{d p_A^3}$ of nuclei with mass number A is connected to the final-state momentum distribution of protons $E_p \frac{d^3 N_p}{d p_p^3}$ via the coalescence parameter [71]:

$$B_A = E_A \frac{d^3 N_A}{d p_A^3} \left(E_p \frac{d^3 N_p}{d p_p^3} \right)^{-A}, \quad (1)$$

assuming that protons and neutrons are produced in equal amounts at ultrarelativistic collision energies since both belong to the same isospin doublet. The coalescence prescription can thus be employed to deduce the formation of nuclei based on measured proton yields as well as on nucleon distributions from event generators such as PYTHIA [74, 75] and EPOS [76], or transport models like UrQMD [77–79] or SMASH [80–82].

In pertinent formulations of the coalescence model, the coalescence probability incorporates a dependence on the spatial distribution of the nucleons at kinetic freeze-out and its overlap with the internal

¹Centrality in heavy-ion collisions is normally given in the inverse percentage of the overlap between the area of the collided nuclei, i.e. 0–10% central collisions corresponds to the events where the collisions are mostly head-on and 80–90% would be a peripheral collision where the colliding nuclei only have a small overlap. Semicentral corresponds to a centrality of 30–50%.

wave function of the nuclear cluster, leading to a characteristic dependence of B_A and consequently the production yield of nuclei on the size of the collision system [83–93]. This motivated detailed studies of nuclear formation in pp, p–Pb, and non-central Pb–Pb collisions, where the yield ratio of nucleus A relative to protons is studied as a function of the average charged-particle multiplicity per unit of pseudorapidity, $\langle dN_{\text{ch}}/d\eta \rangle$. Indeed, the present data tend to confirm the system-size dependence predicted by coalescence models for the yield ratios deuteron to proton (d/p), triton to proton (t/p), and ^3He to proton ($^3\text{He}/\text{p}$) in small collision systems [41, 43–46, 48–50]. On the other hand, the statistical description of particle production in small collision systems requires a canonical formulation of the statistical hadronization model, leading to the Canonical Statistical Model (CSM). This formulation entails an additional model parameter, the so-called correlation volume V_C , inside which electric charge Q , strangeness S , and baryon number B are conserved exactly [63, 64, 94–97]. CSM calculations of nucleus-to-proton ratios result in a suppression of the production of nuclei in small systems that is qualitatively compatible with the patterns observed in data, but still tends to overestimate the yields of nuclei for realistic assumptions of V_C [52, 63, 96].

In central and semi-central Pb–Pb collisions, recent results for d/p and $^3\text{He}/\text{p}$ are compatible with both statistical hadronization and coalescence models, while t/p in Pb–Pb is significantly closer to the coalescence model [54]. It should be noted, however, that the yield of nuclei in Pb–Pb collisions may also be modified by absorption effects during the hadronic phase, as indicated by calculations from the UrQMD hybrid coalescence model [79].

The observed stiffening of transverse-momentum (p_T) spectra of hadrons produced in heavy-ion collisions can be interpreted in terms of a common radial flow field, arising from hydrodynamic expansion. The so-called blast-wave model [98] describes the radial boost of the light-flavor hadrons and nuclei arising from hydrodynamic expansion with a common set of parameters: the kinetic freeze-out temperature T_{kin} , the mean radial expansion velocity $\langle \beta \rangle$, and an exponent n of the radial velocity profile. The measured p_T spectra are fitted with the Boltzmann-Gibbs blast-wave function [98]:

$$E \frac{d^3N}{dp^3} \propto \int_0^R m_T I_0 \left(\frac{p_T \sinh(\rho(r))}{T_{\text{kin}}} \right) K_1 \left(\frac{m_T \cosh(\rho(r))}{T_{\text{kin}}} \right) r dr \quad (2)$$

where m_T is the transverse mass ($m_T = \sqrt{m^2 + p_T^2}$), I_0 and K_1 are the modified Bessel functions, and ρ is the velocity profile given by:

$$\rho(r) = \tanh^{-1} \beta(r) = \tanh^{-1} \left[\left(\frac{r}{R} \right)^n \beta_{\text{max}} \right], \quad (3)$$

where r is the radial distance in the transverse plane, R is the radius of the fireball and β_{max} is the transverse expansion velocity at the surface of the expanding fireball.

The study of (anti)alpha production in central Pb–Pb collisions is particularly interesting because it is the heaviest nucleus measured at the LHC so far. In the SHM, there is a strong mass dependence of the statistical penalty factor (yield suppression when a baryon is added to the system) for typical values of T_{ch} and μ_B , while predictions of coalescence models depend on nucleon densities and geometrical factors to the power of A . For the SHM the antialpha-to-alpha ratio is expected to be proportional to $\exp(-8\mu_B/T_{\text{ch}})$ [99], which is the strongest dependence of the thermal model parameters on the baryon number A . The microscopic coalescence models directly have problems to get the predictions, since they need much more nucleons to be produced initially that can be used then in the coalescence process. This makes the (anti)alpha a very sensitive probe for stringent tests of the production models of light nuclei. In addition to already discussed models, there is also the idea that correlations are present already in the vacuum, allowing an antinucleus like antialpha to be directly excited from the vacuum [100–103].

This would mean that the antinuclei rate could be much larger than the values predicted by SHM or coalescence models, which expect them to be rather equal. Previous measurements of the integrated yields of antialpha and alpha in central Pb–Pb collisions at a center-of-mass energy per nucleon–nucleon pair of $\sqrt{s_{NN}} = 2.76$ TeV agreed with a global fit of the SHM to the yields of all measured hadrons and nuclei [42]. No predictions for $A = 4$ from coalescence models existed at the time.

In this letter, we present results on (anti)alpha production in central Pb–Pb collisions at $\sqrt{s_{NN}} = 5.02$ TeV, including the first ever measured transverse-momentum spectrum of the antialpha. The results are compared to predictions by coalescence and statistical hadronization models. Together with previous results for different hadron species and lighter nuclei, the p_T spectra are analyzed employing the blast-wave model. Throughout this letter, especially in the figures but also at some occasions in the text, ${}^4\text{He}$ instead of alpha is stated, which are used as equivalent. Note that with ${}^4\text{He}$ not the chemical element with electron shell but the ${}^4\text{He}$ nucleus is meant.

In Sec. 2 the analysis is described, followed by the presentation of the systematic uncertainties in Sec. 3. The results are discussed in Sec. 4 and the conclusion is given in Sec. 5.

2 Data analysis

2.1 Data sample and experimental apparatus

The presented results are based on a data set of Pb–Pb collisions at $\sqrt{s_{NN}} = 5.02$ TeV, collected in 2018, where 99.5×10^6 events in the 0–10% centrality interval [104] were analyzed. These events are the sum of a minimum-bias trigger of lower bandwidth and a central trigger with a higher bandwidth, giving 12.6×10^6 and 86.9×10^6 events, respectively. The number of antialpha candidates outside the chosen interval is negligible and would not give any statistical benefit.

The ALICE apparatus [105, 106] provides excellent particle identification and vertexing capabilities. The (anti)alpha was reconstructed and identified using the Inner Tracking System (ITS), the Time Projection Chamber (TPC), the Transition Radiation Detector (TRD), and the Time-Of-Flight detector (TOF). These detectors are all located inside a homogeneous magnetic field with a strength of 0.5 T and cover the full azimuth in the pseudorapidity range $|\eta| < 0.9$. Interactions located inside $|z| < 10$ cm are selected, where z is the distance from the nominal interaction point along the beam direction.

The ITS [107] is a silicon detector consisting of six cylindrical layers. It is used for charged-particle tracking and for the reconstruction of primary and secondary vertices. It can also be used to separate primary nuclei from secondary, knocked-out nuclei from the detector material, via the distance of closest approach (DCA) of the track to the primary vertex.

The TPC [108] is the main tracking device of the ALICE apparatus. It is a gas-filled cylinder and provides charged-particle tracking and particle identification via the specific energy loss per path length (dE/dx) with a resolution of 6% in Pb–Pb collisions.

The TOF detector [109] provides identification of light (anti)nuclei by means of the velocity determination from the calculated path length of the track and the time-of-flight measurement. Its total time resolution for tracks in Pb–Pb collisions corresponds to about 65 ps which is determined by the intrinsic time resolution of the detector and the resolution of the event collision time measurement. By combining TPC and TOF information, (anti)alphas can be identified from $p_T = 2$ GeV/ c up to 6 GeV/ c in Pb–Pb collisions.

The TRD [110] can be used to improve the momentum resolution and significantly reduces the probability of random matches between tracks and TOF hits.

The V0 detectors [111] measure the arrival time of particles with a resolution of 1 ns, by utilizing a

pair of forward and backward scintillator arrays (covering the pseudorapidity ranges $2.8 < \eta < 5.1$ and $-3.7 < \eta < -1.7$). They are used for triggering purposes and for rejection of beam–gas interactions. In addition, they provide the centrality trigger in Pb–Pb collisions [104], and they are also used for offline centrality determination.

The Zero Degree Calorimeter (ZDC) consists of two sets of hadronic calorimeters, which are located 112.5 m away from the interaction point on both sides of it, and of one set of electromagnetic calorimeters, placed 7 m away from the interaction point [105] on one side of it. It is located at 0° relative to the beam direction.

2.2 Event and track selection

The data were collected using a minimum-bias trigger requiring at least one hit in both V0 detectors. In addition, a trigger on central collisions was used, also determined by the V0 detectors, selecting collisions in the 0–10% centrality interval. To reject the events triggered by the interactions of the beam with the residual gas in the LHC vacuum pipe, the timing information of the V0 scintillator arrays is used. A further selection using the ZDC is applied in order to reject the electromagnetic beam–beam interactions and beam–satellite bunch collisions [112]. This is done by selecting good events from the correlation between the sum and the difference of arrival times measured in each of the ZDCs [106]. All these rejection steps are done in the offline analysis.

The production yield of (anti)alphas is measured at midrapidity ($|y| < 0.5$). Only tracks in the full tracking acceptance of $|\eta| < 0.8$ are selected. In order to guarantee good track momentum and dE/dx resolution in the relevant p_T ranges, the selected tracks are required to have at least 70 out of 159 possible reconstructed points in the TPC and at least two points in the ITS out of which at least one is in the two innermost layers, the Silicon Pixel Detector (SPD). The requirement of at least one point in the SPD assures a resolution better than $300 \mu\text{m}$ on the distance of closest approach to the primary vertex for the selected tracks [106]. Furthermore, it is required that the χ^2 per TPC reconstructed point is less than 2.5 and tracks with a kink, which originate from weak decays, where the decay products are one charged and at least one neutral particle, are rejected.

2.3 Particle identification

Particles with electric charge $z = 2$ are well separated in the TPC from the particles with $z = 1$, as they have a four times larger specific energy loss (dE/dx). However, to distinguish the alphas from the much more abundant ^3He (by a factor of the order of 10^3) the dE/dx information is combined with the mass calculated from the time-of-flight measured with the TOF and the track momentum. The energy loss in the TPC can be described by the Bethe–Bloch formula for a given mass hypothesis. To select the (anti)alphas it is required that the energy loss of the track lies in a 3σ window around the expected values for alpha particles, where σ is the dE/dx resolution. In addition, it is required that the track is matched to a hit in the TOF detector. Figure 1 shows the m^2/z^2 distribution of the TOF detector for antialpha candidates (green) in the p_T interval between 3 and 6 GeV/c. The m^2/z^2 for true (anti)alphas is $3.475 \text{ GeV}^2/c^4$. Note that in the m^2/z^2 distributions, ^4He are clearly separated from ^3He , for which m^2/z^2 is $2.0 \text{ GeV}^2/c^4$. The background (magenta) is coming from TOF mismatches, which is the case if a track in the TPC is associated with the wrong hit in the TOF detector, resulting in a wrong mass. To describe the background a data-driven approach with only one free parameter is used. The background is determined by selecting all tracks in the TPC outside a 3σ interval of the expected Bethe–Bloch curve for alpha particles and in addition outside a 3σ interval of the expected curve for the deuteron mass hypothesis, as alphas and deuterons have similar m^2/z^2 . The background is then scaled to the height of the ^4He histogram by normalizing to the sideband on the right of the ^4He peak between 4.4 and $6 \text{ GeV}^2/c^4$ and subtracted. This is done in each p_T interval separately except for the first p_T interval of the ^4He ($2\text{--}3 \text{ GeV}/c$), where there is no background. The ^3He contribution under the ^4He peak is

described by an exponential fit to the tail of the ${}^3\text{He}$ peak (blue dashed line). This is done in one p_T interval from 3 to 6 GeV/c and an (anti) ${}^3\text{He}$ fraction (3% for ${}^3\bar{\text{He}}$ and 9% for ${}^3\text{He}$) is determined for particles and antiparticles separately, which is then subtracted in each p_T interval individually. This is needed since the ${}^3\text{He}$ contribution cannot be determined in each p_T interval separately due to the limited statistics. The (anti)alpha signal is counted in every p_T interval between 3 and 4.2 GeV $^2/c^4$ due to the asymmetric shape of the signal in m^2/z^2 .

The ${}^4\bar{\text{He}}$ raw yield is extracted in four p_T intervals between 2 and 6 GeV/c. The ${}^4\text{He}$ raw yield is only extracted in three p_T intervals between 3 and 6 GeV/c, due to the large contribution of knocked-out alphas from the detector material and the support structure at low p_T . This contribution can only be extracted properly from data to Monte Carlo comparison and is done usually in template fits in slices of p_T in the variable distance-of-closest approach. Unfortunately, this extraction is not possible for the presented analysis due to the small number of candidates. Nevertheless, the comparison of the raw counts in p_T intervals suggests that the knock-out is negligible already for $p_T > 3$ GeV/c, since the raw yields of alpha and antialpha become similar in number. For the statistical uncertainties of the data points the Poisson statistics is used.

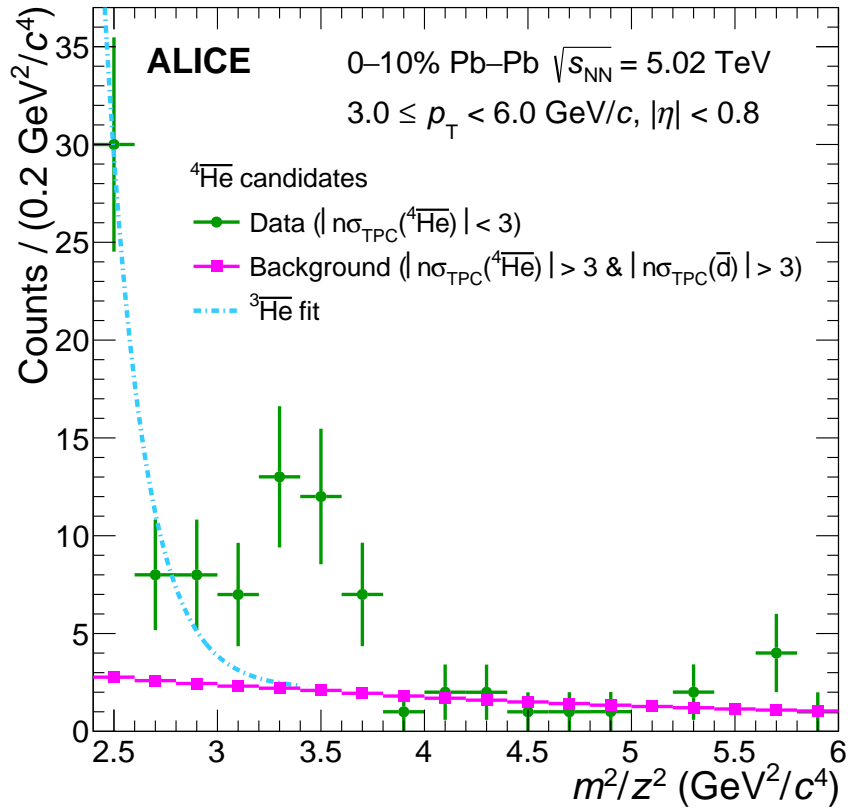


Figure 1: (Color online) m^2/z^2 distribution for ${}^4\bar{\text{He}}$ candidates (green). The background (magenta) is constructed by selecting all candidates outside the ${}^4\bar{\text{He}}$ TPC window of 3σ around the alpha mass hypothesis ($|n\sigma_{\text{TPC}}({}^4\bar{\text{He}})| > 3$) and in addition outside the 3σ window around the deuteron mass hypothesis ($|n\sigma_{\text{TPC}}(\bar{d})| > 3$). The blue line is an exponential fit to the rise at lower masses originating from ${}^3\bar{\text{He}}$ candidates.

2.4 Corrections to the spectra

The transverse-momentum spectra of the (anti)alphas are obtained by correcting the raw yields in the different p_T intervals of the analysis for tracking efficiency and detector acceptance. This is done by using Monte Carlo events, simulated with the HIJING event generator [113]. As HIJING does not include

(anti)alphas, they are injected into the event with flat distributions in p_T (between 0 and 10 GeV/ c), azimuth (between 0 and 2π), and rapidity ($|y| < 1$). The GEANT4 [114] transport code is used to propagate the generated particles through a full simulation of the ALICE detector setup. The combined acceptance \times efficiency was determined for the (anti)alphas in the 0–10% centrality interval. As the nuclei are not produced with flat p_T distribution, the acceptance \times efficiency was weighted with a blast-wave shape applying an iterative method (see e.g. Ref. [54]), where the blast-wave parameters were taken from a fit to the (anti)alpha spectra.

3 Systematic uncertainties

To estimate the systematic uncertainties, different sources affecting the (anti)alpha measurement were studied, which are described in the following. Unless specified otherwise, all uncertainties are taken for all p_T intervals equally.

The first considered source of systematic uncertainty is related to possible imperfections in the description of the track reconstruction efficiency in the Monte Carlo simulations, which is usually estimated by varying the track selection criteria and by comparing the probability of attaching ITS hits to a TPC track (matching efficiency) in the data and in the simulation. Owing to the low number of counts of the (anti)alpha analysis the systematic variations of the track selection criteria were found to be not significant within the statistical uncertainties by applying the check proposed by Barlow [115]. Therefore, the method based on varying the selections could not be used and instead systematic uncertainties based on similar studies of identified charged particles were assigned, namely 5% for the TPC–ITS matching efficiency for all p_T intervals [116].

For the signal extraction, a systematic uncertainty between 6% and 22% for the ${}^4\overline{\text{He}}$ and between 9% and 14% for the ${}^4\text{He}$ has been evaluated. This uncertainty takes into account variations in fit functions and fit ranges used for yield extraction.

The limited knowledge of the interaction of (anti)nuclei with the detector material leads to another large contribution to the systematic uncertainties. The hadronic interaction cross section implemented in GEANT4 [114, 117–119] is used to determine the acceptance \times efficiency. As there is no measurement of the ${}^4\overline{\text{He}}$ inelastic interaction cross section so far, an uncertainty of 7% is assumed, as done for the ${}^4\overline{\text{He}}$ measured in the Pb–Pb data sample at $\sqrt{s_{\text{NN}}} = 2.76$ TeV [42]. The 7% are supposed to cover the difference between GEANT4, which was used for the propagation of the tracks in the detector material, and the true interaction cross sections [42]. This uncertainty represents the difference between the cross section implemented in GEANT4 to the one implemented in the AMS model in the rigidity interval where ALICE and AMS measurements overlap.

The material budget of the ALICE apparatus employed in the MC simulation was varied by $\pm 4.5\%$, corresponding to the uncertainty of the ALICE material budget determination [106]. This results in an uncertainty on the (anti)alpha spectra of 2%.

The blast-wave weighting of the acceptance \times efficiency only affects the first p_T interval of the ${}^4\overline{\text{He}}$ spectrum and the uncertainty was determined to be 3%. This is half of the difference to the case when no blast-wave weighting is taken into account.

As there is a contribution of feed-down to the (anti)alphas from the decay of ${}^4_{\Lambda}\text{H}$ and ${}^4_{\Lambda}\overline{\text{H}}$, an additional uncertainty of 3% for particles and antiparticles in all p_T intervals was taken into account, estimated from a Monte Carlo study where these hypernuclei have been injected.

In total, all these contributions result in a systematic uncertainty between 12% and 24% for ${}^4\overline{\text{He}}$ and between 12% and 16% for ${}^4\text{He}$ when added in quadrature.

Most of the systematic uncertainties are correlated between ${}^4\text{He}$ and ${}^4\overline{\text{He}}$. The uncorrelated contributions

are the uncertainty coming from the inelastic interaction cross section as well as the uncertainties on the background subtraction and the (anti) ^3He contribution, which are part of the signal extraction.

4 Results

The size of the data sample presented in this letter exceeds that of a previous measurement in Pb–Pb collisions at $\sqrt{s_{\text{NN}}} = 2.76$ TeV [42] by about a factor of five. This allows for the determination of the transverse-momentum spectra for alpha and antialpha, as shown in Fig. 2. In the case of the antialpha, this is the first ever measurement of the p_{T} distribution. In the p_{T} interval between 4 and 5 GeV/c there is a 2σ discrepancy between particle and antiparticle yields, relative to the combination of statistical and systematic uncertainties, while in the other p_{T} intervals the alpha and antialpha yields are consistent within statistical uncertainties. The antialpha-to-alpha ratio is shown in the lower panel of Fig. 2, where the error bars represent the statistical uncertainties and the boxes represent the uncorrelated systematic uncertainties, as the correlated ones cancel. Both spectra were combined for further analysis by constructing the weighted average of the data points, where statistical and systematic uncertainties were considered.

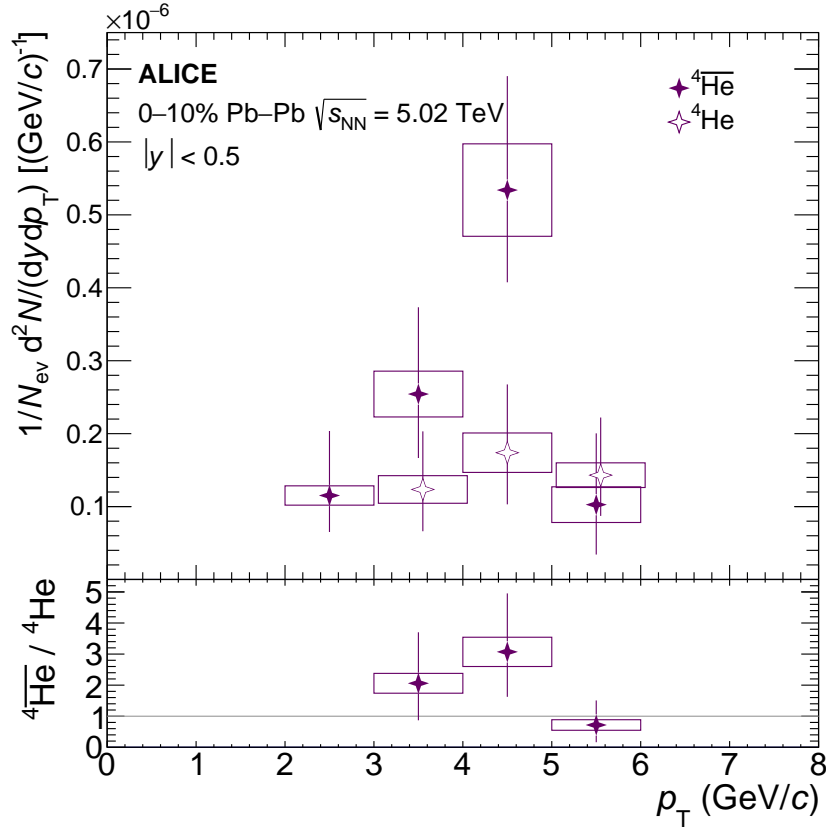


Figure 2: Measured transverse-momentum distributions of ^4He and $^4\bar{\text{He}}$ (upper panel). The vertical lines indicate the statistical uncertainties, while the boxes represent the systematic ones. In the case that the statistical uncertainties would overlap the $^4\bar{\text{He}}$ points are a bit shifted on the x-axis. The lower panel shows the ratio between $^4\bar{\text{He}}$ and ^4He with statistical and uncorrelated systematic uncertainties as the correlated systematic uncertainties cancel.

The combined (anti)alpha p_{T} spectrum was compared to those of other light-flavored hadrons [116] and nuclei [54], measured in central (0-10%) Pb–Pb collisions at $\sqrt{s_{\text{NN}}} = 5.02$ TeV, by performing a simultaneous blast-wave fit to all p_{T} spectra (see Fig. 3, left). The fit range of π , K, p was restricted in the momentum range in order to minimize biases from resonance decays at low p_{T} and from hard

processes at high p_T . The fit is performed in the following p_T intervals: 0.5–1 GeV/c for charged pions, 0.2–1.5 GeV/c for charged kaons, and 0.3–3 GeV/c for (anti)protons. These regions are the same as in the previous publications that showed results for global blast-wave fits [41, 116, 120]. The spectra of antideuterons, antitritons, ${}^3\overline{\text{He}}$, and alpha were fitted over the full measured p_T range.

One should note, blast-wave fits are a simplified approach mimicking the hydrodynamics behind the radial expansion and have certain limitations, e.g. it is known that the temperature is particularly sensitive to the fit range and the used particle species. In particular, in blast-wave fits using the FastReso package [121, 122] the quality of the fits is rather good using a single temperature of about 150 MeV for chemical and kinetic freeze out and these fits do not show a dependence of the temperature on centrality [123]. This is possible in the FastReso approach because the feed-down from resonances is taken into account by the package. In addition, there are other approaches utilizing results from LHC that can describe the data in an extended blast-wave model approach with more parameters [124]. In any case, the standard (Boltzmann-Gibbs) blast-wave fit provides a simple and solid approach to compare the spectra of nuclei and lighter hadrons, which is the goal of the study presented here.

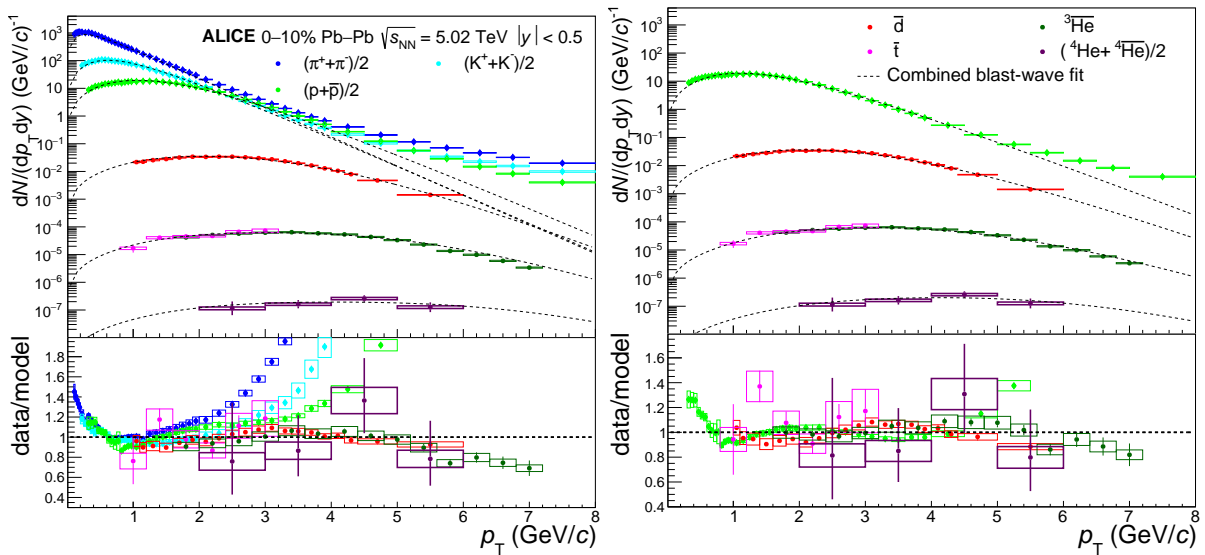


Figure 3: (Color online) Combined blast-wave fit of all available light flavored hadron p_T spectra including nuclei [54, 116] (left) and only p , \bar{d} , \bar{t} , ${}^3\overline{\text{He}}$ and ${}^4\text{He}$ p_T spectra (right) in Pb–Pb collisions at $\sqrt{s_{\text{NN}}} = 5.02$ TeV for 0–10% central events (upper panels). The lower panels show the ratio between each data point and the blast-wave model fit for each species.

The fit results are shown in the left panel of Fig. 3 and the fit parameters are reported in Table 1 (Fit A). The freeze-out parameters, in particular $\langle\beta\rangle$ and T_{kin} , are consistent with those obtained in Pb–Pb collisions at $\sqrt{s_{\text{NN}}} = 2.76$ TeV [41]. The data-to-model ratios, shown in the bottom panel of Fig. 3 left, indicate that the spectra of nuclei are reasonably well described by the common fit within their uncertainties. This suggests that also relatively heavy compound objects like (anti)alpha nuclei participate in a common flow field.

The coalescence picture assumes that nuclei are formed at a late stage of the collision, i.e. at or after kinetic freeze-out. In this case, one may expect that the p_T spectra of protons and (anti)nuclei exhibit a common temperature and velocity field that characterizes the source at or after the stage of nuclear cluster formation. To elucidate this further a blast-wave fit was performed, where only protons and (anti)nuclei are included (Fit B). The data points are well described by the common fit, as shown in Fig. 3 (right). Actually, the protons are well described over a larger range in Fit B (right panel of Fig. 3) than in Fit A. The fit parameters indicate a similar velocity field as in the case when π and K are

Table 1: Parameters obtained from the combined blast-wave fits (Fig. 3) to the p_T spectra of different combinations of light-flavor hadrons and nuclei measured in central (0–10%) Pb–Pb collisions at $\sqrt{s_{NN}}=5.02$ TeV. The uncertainty from the fits corresponds to the statistical uncertainty. Systematics, that have been evaluated by changing the fit strategy slightly, are of similar size as the statistical uncertainties. The last column shows the χ^2 value and the corresponding number of degrees of freedom (ndf) for each fit.

	Fitted particles	$\langle\beta\rangle$	β_{\max}	T_{kin} (MeV)	n	χ^2/ndf
Fit A	$\pi, K, p, d, t, {}^3\text{He}, {}^4\text{He}$	0.664 ± 0.002	0.873 ± 0.004	108 ± 2	0.63 ± 0.02	381.1 / 92
Fit B	$p, d, t, {}^3\text{He}, {}^4\text{He}$	0.670 ± 0.002	0.853 ± 0.004	132 ± 4	0.55 ± 0.02	176.5 / 64
Fit C	$d, t, {}^3\text{He}, {}^4\text{He}$	0.684 ± 0.003	0.863 ± 0.005	108 ± 6	0.52 ± 0.02	44.5 / 37
Fit D	π, K, p	0.664 ± 0.002	0.909 ± 0.003	85 ± 4	0.74 ± 0.01	113.0 / 54

included in the fit (Fit A), but a significantly larger kinetic freeze-out temperature of $T_{\text{kin}} = (132 \pm 4)$ MeV. In the context of final-state coalescence, this finding is unexpected. However, it matches the conjecture of statistical hadronization including formation of (anti)nuclei close to the phase boundary, without significant rescattering at later stages of the system evolution. Possible explanations for such a scenario in terms of pre-hadronic multi-quark states have been proposed in Ref. [62].

The result is challenged by a fit to only the (anti)nuclei (Fit C) which yields $T_{\text{kin}} = (108 \pm 6)$ MeV, which is consistent within the uncertainties with the result of Fit A. This seems to be more in agreement with the expectation of the coalescence model, namely that the protons freeze out earlier as suggested by Fit B, i.e. at a higher temperature, and the nuclei are formed later from these protons and neutrons available for the coalescence process. A fit to only π, K, p (Fit D) results in $T_{\text{kin}} = (85 \pm 4)$ MeV, indicating that very low apparent kinetic freeze-out temperatures are driven by the lightest particles. It should be noted that lighter particles are more prone to contributions from resonance decays and hard scatterings over a wider p_T range than heavier particles.

From the quality of the fits, i.e. the χ^2/ndf values given in Table 1, it seems like the separation into nuclei (Fit C) and light-flavored hadrons (Fit D) is best. Nevertheless, the temperature of the latter is lower than Fit C, so the coalescence picture is again questioned from this inconsistency between blast-wave results. Indeed, the temperatures extracted from the fits would imply that the protons used in the coalescence process freeze out later than the nuclei formed from them.

Clearly, these findings cannot be used for any strong conclusion, in particular since the blast-wave model is only a simplified hydrodynamical picture that has certain limits as discussed above.

The rapidity densities dN/dy are estimated by integration over the blast-wave function fitted to the limited range of p_T spectra. To this end, a blast-wave fit was performed to the p_T spectra of all particles except (anti)alpha. The resulting fit parameters are used to constrain the shape for (anti)alpha while the normalization is obtained by a fit to the (anti)alpha distributions. This procedure was applied separately for the alpha and antialpha p_T distributions as well as to the combined spectrum. The derived rapidity densities are summarized in Table 2. The statistical uncertainties are those of the normalization from the fit, while the systematic uncertainties reflect the variation of dN/dy if the data points are shifted by their systematic uncertainties. The results for alpha and antialpha are consistent within their uncertainties. Also reported are the SHM results obtained from a fit of all available hadron yields using a grand-canonical ensemble [60, 63, 125].

Table 2: Rapidity densities of ${}^4\text{He}$ and ${}^4\overline{\text{He}}$ and their average, together with the statistical hadronization model predictions [60, 63, 125]. The experimental values are stated with statistical (second value) and systematic uncertainties (third value).

dN/dy (10^{-6}):	${}^4\overline{\text{He}}$	${}^4\text{He}$	$({}^4\overline{\text{He}} + {}^4\text{He})/2$
Experiment	$(1.30 \pm 0.28 \pm 0.18)$	$(0.83 \pm 0.22 \pm 0.12)$	$(1.00 \pm 0.19 \pm 0.10)$
SHM ($T_{\text{ch}} = 156$ MeV)	0.945	0.949	0.947

The presented (anti)alpha transverse-momentum spectra allow for the first time a determination of the coalescence parameter B_4 at LHC energies. To this end, Eq. 1 was employed where the proton p_T distributions were taken from Ref. [116] after averaging the measurements in the 0–5% and 5–10% centrality intervals. The B_4 values shown in Fig. 4 exhibit an increasing trend with p_T/A , which is the transverse momentum per nucleon. This trend is similar to earlier measurements in heavy-ion collisions for lighter nuclei [41, 54]. The results in Fig. 4 are compared to predictions from coalescence [92] and from statistical hadronization models. For the latter, the (anti)alpha and proton yields (dN/dy) are calculated for a chemical freeze-out temperature of $T_{\text{ch}} = 156$ MeV and the shapes of the transverse-momentum distributions are taken from the blast-wave fit. While SHM, combined with the spectral shape derived from the blast-wave fit, slightly underpredicts the data, the coalescence prediction is about one order of magnitude below the data in all p_T intervals. However, both models capture the increase of the data well. So intrinsically, the spectral shape seems to be correct in both approaches and the magnitude of the discrepancy between the coalescence curve and the data needs to be understood better.

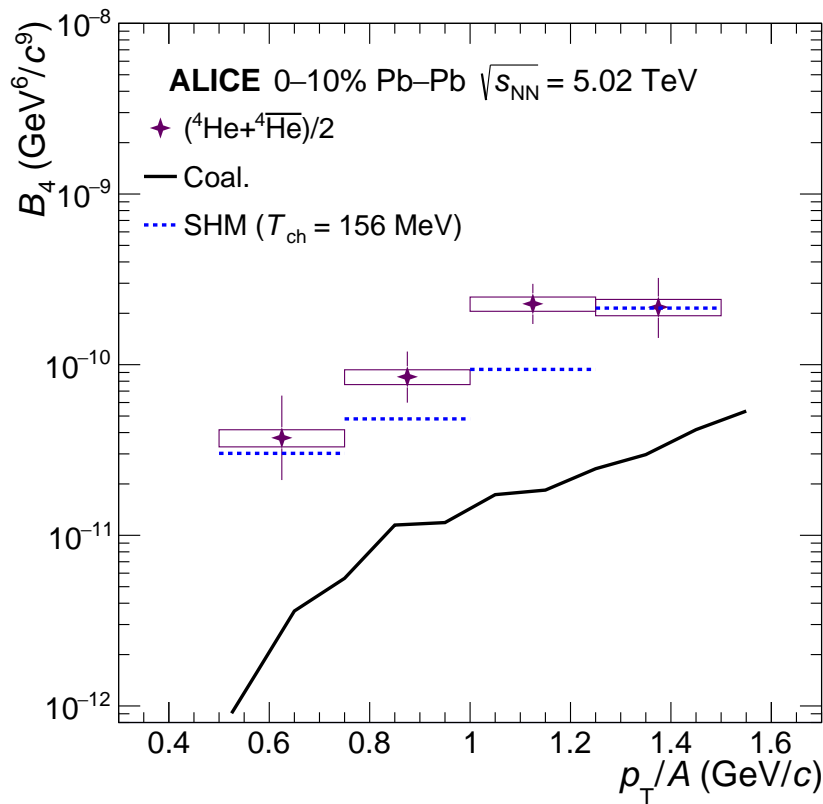


Figure 4: (Color online) The coalescence parameter B_4 as a function of p_T/A , calculated from the averaged ${}^4\text{He}$ and ${}^4\overline{\text{He}}$ spectra and the protons from [116]. Statistical uncertainties are indicated by the vertical lines and the boxes correspond to the systematic uncertainties. The blue dashed line and the full black line indicate the values for the SHM combined with blast-wave p_T shapes and the coalescence predictions from Refs. [91, 92], respectively.

The ratio of alpha to proton dN/dy in central Pb–Pb collisions at $\sqrt{s_{\text{NN}}} = 5.02$ TeV is shown in Fig. 5 as a function of the pseudorapidity density of charged particles produced at midrapidity in the collision, $\langle dN_{\text{ch}}/d\eta \rangle_{|\eta_{\text{lab}}| < 0.5}$. In addition, the ratio from the 10% most central Pb–Pb collisions at $\sqrt{s_{\text{NN}}} = 2.76$ TeV [42] and the upper limit in p–Pb collisions at $\sqrt{s_{\text{NN}}} = 5.02$ TeV [126] are depicted. The new result agrees well with the measurement at lower energy [42]. Furthermore, predictions from the canonical statistical model (CSM) for $T_{\text{ch}} = 155$ MeV and three different values of the correlation volume V_C are displayed [63]. The curves differ at low $\langle dN_{\text{ch}}/d\eta \rangle$, corresponding to the multiplicity of charged particles produced in small collision systems, but coincide in central Pb–Pb collisions where they are consistent

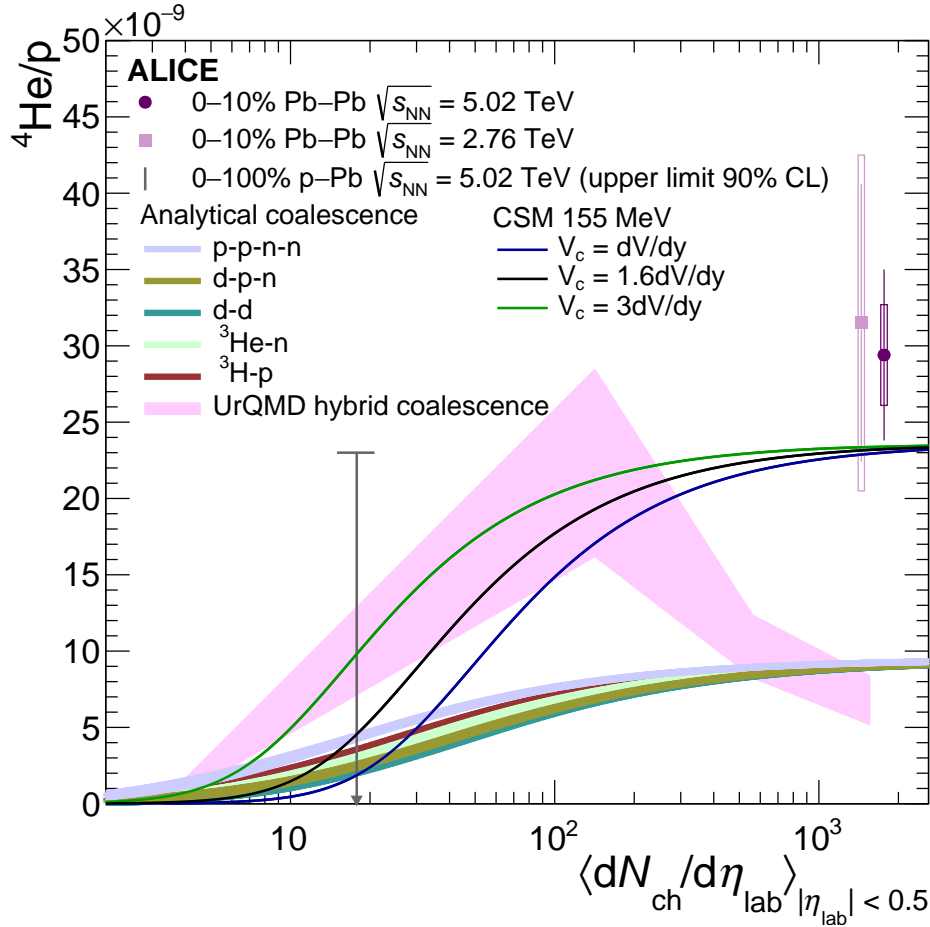


Figure 5: (Color online) ${}^4\text{He}/p$ ratios for the measured data points as a function of charged-particle multiplicity $\langle dN_{ch}/d\eta \rangle_{|\eta_{lab}| < 0.5}$ compared to model predictions. For comparison the result from the 10% most central Pb–Pb collisions at $\sqrt{s_{NN}} = 2.76$ TeV [42] and the upper limit at 90% CL from p–Pb collisions at $\sqrt{s_{NN}} = 5.02$ TeV [126] is also shown. The thermal model curves are from the CSM [63]. For the coalescence model two different approaches are displayed: analytical and UrQMD hybrid coalescence [127, 128]. The analytical coalescence is shown for five different substructures and the thickness of the bands reflects the uncertainties of the calculation. For the UrQMD model the band is representing the statistical uncertainty of the prediction.

within uncertainties with the measurements. Also shown are different calculations from coalescence models. The “box coalescence” (using a maximal difference in coordinate space and momentum for the coalescing partners) implemented in the UrQMD [79] model, indicated by the magenta band, shows a non-monotonic behavior that can be explained by absorption processes in the hadronic phase of Pb–Pb collisions [127]. In central Pb–Pb collisions, the UrQMD hybrid model underestimates the data by about a factor of three. The same trend is observed in a CSM approach that includes annihilations [68], which also underestimates the data. Finally, calculations of an analytical coalescence approach are presented, in which the internal structure of the alpha nucleus is taken into account [128]. The assumption of a structureless alpha particle (p-p-n-n) and calculations considering a d-p-n, d-d, ${}^3\text{H-p}$ or ${}^3\text{He-n}$ substructures are compared. All analytical coalescence curves coincide for large system sizes where they underestimate the data by about a factor of three. This might be connected to the fact that the binding energy of the alpha is not taken into account in the model. Neglecting the binding energy might be working well for the $A = 2$ and $A = 3$ nuclei, but not for the alpha, since it is much tighter bound compared to lighter nuclei ($E_B = 2.2$ MeV for the deuteron, whereas the alpha is bound by 28.3 MeV). A recent publication determined the mass radius of the alpha to be (1.70 ± 0.14) fm in a model dependent approach using

$\phi(1020)$ -photoproduction data, that is close to the measured charge radius which is not expected [129]. The mass radius of the alpha used in the coalescence calculations is rather 1.4 fm, estimated from the measured charge radius of (1.6755 ± 0.0028) fm [92, 130]. In fact, there is a more precise measurement of the charge radius using laser spectroscopy of muonic helium ions, that gives (1.67824 ± 0.00083) fm [131]. It should be noted that, the presented data even allows for the sum of contributions from coalescence and statistical hadronization predictions. Since these processes are not mutually exclusive one could actually imagine it as interplay of these two production mechanisms.

5 Conclusion

New results on (anti)alpha production in central Pb–Pb collisions at $\sqrt{s_{\text{NN}}} = 5.02$ TeV were presented, including the first differential measurement of the antialpha transverse-momentum distribution. Predictions from statistical hadronization models are compatible with the measured coalescence parameters B_4 and the (anti)alpha-to-proton yield ratio. In contrast, different implementations of the coalescence model underestimate the data significantly. These findings for the production of (anti)alpha are different from the results for $A = 3$ nuclei [54], where both classes of models differ only by about 30% and the data tend to lie in between. Improvements for the models, e.g. incorporating the binding energy of the alpha, are needed to get a better understanding of its production. A blast-wave analysis of the p_T distributions together with other hadrons and light nuclei from central Pb–Pb collisions suggests that also relatively heavy compound objects like (anti)alpha nuclei participate in a common flow field. However, the constraint of the (anti)alpha on this is limited by the current statistics. On the other hand, a blast-wave fit including only protons and light nuclei up to ${}^4\text{He}$ results in a kinetic freeze-out temperature that is rather close to the chemical freeze-out temperature obtained from statistical hadronization models. Note that one should be careful with any strong conclusion from the blast-wave fit, since it has certain limitations, e.g. being sensitive on the fit regions and the treatment of feed-down from resonances. Nevertheless, this result does not agree with naïve expectations based on the coalescence picture, but is in line with a scenario where the yields of light nuclei in central Pb–Pb collisions are dominated by thermal production close to the QCD phase boundary. It should be noted that thermal production and coalescence are not mutually exclusive processes and that the data presented here are even compatible with the sum of contributions from coalescence and statistical hadronization, suggesting a possible interplay of these two production mechanisms.

The recent upgrades of the ALICE detector will enable the collection of substantially larger data samples during LHC Runs 3 and 4. This will allow for more differential measurements of (anti)alpha production, enabling in particular a systematic study of its dependence on multiplicity and collision system size. The large sensitivity of the (anti)alpha yield to the different production scenarios may help to shed light on the interplay between coalescence and thermal production and a possible transition between them at intermediate system sizes.

Acknowledgements

We thank J. Steinheimer and K.-J. Sun for useful discussions and for providing their predictions.

The ALICE Collaboration would like to thank all its engineers and technicians for their invaluable contributions to the construction of the experiment and the CERN accelerator teams for the outstanding performance of the LHC complex. The ALICE Collaboration gratefully acknowledges the resources and support provided by all Grid centres and the Worldwide LHC Computing Grid (WLCG) collaboration. The ALICE Collaboration acknowledges the following funding agencies for their support in building and running the ALICE detector: A. I. Alikhanyan National Science Laboratory (Yerevan Physics Institute) Foundation (ANSL), State Committee of Science and World Federation of Scientists (WFS), Armenia; Austrian Academy of Sciences, Austrian Science Fund (FWF): [M 2467-N36] and National-

stiftung für Forschung, Technologie und Entwicklung, Austria; Ministry of Communications and High Technologies, National Nuclear Research Center, Azerbaijan; Conselho Nacional de Desenvolvimento Científico e Tecnológico (CNPq), Financiadora de Estudos e Projetos (Finep), Fundação de Amparo à Pesquisa do Estado de São Paulo (FAPESP) and Universidade Federal do Rio Grande do Sul (UFRGS), Brazil; Bulgarian Ministry of Education and Science, within the National Roadmap for Research Infrastructures 2020-2027 (object CERN), Bulgaria; Ministry of Education of China (MOEC), Ministry of Science & Technology of China (MSTC) and National Natural Science Foundation of China (NSFC), China; Ministry of Science and Education and Croatian Science Foundation, Croatia; Centro de Aplicaciones Tecnológicas y Desarrollo Nuclear (CEADEN), Cubaenergía, Cuba; Ministry of Education, Youth and Sports of the Czech Republic, Czech Republic; The Danish Council for Independent Research | Natural Sciences, the VILLUM FONDEN and Danish National Research Foundation (DNRF), Denmark; Helsinki Institute of Physics (HIP), Finland; Commissariat à l’Energie Atomique (CEA) and Institut National de Physique Nucléaire et de Physique des Particules (IN2P3) and Centre National de la Recherche Scientifique (CNRS), France; Bundesministerium für Bildung und Forschung (BMBF) and GSI Helmholtzzentrum für Schwerionenforschung GmbH, Germany; General Secretariat for Research and Technology, Ministry of Education, Research and Religions, Greece; National Research, Development and Innovation Office, Hungary; Department of Atomic Energy Government of India (DAE), Department of Science and Technology, Government of India (DST), University Grants Commission, Government of India (UGC) and Council of Scientific and Industrial Research (CSIR), India; National Research and Innovation Agency - BRIN, Indonesia; Istituto Nazionale di Fisica Nucleare (INFN), Italy; Japanese Ministry of Education, Culture, Sports, Science and Technology (MEXT) and Japan Society for the Promotion of Science (JSPS) KAKENHI, Japan; Consejo Nacional de Ciencia (CONACYT) y Tecnología, through Fondo de Cooperación Internacional en Ciencia y Tecnología (FONCICYT) and Dirección General de Asuntos del Personal Académico (DGAPA), Mexico; Nederlandse Organisatie voor Wetenschappelijk Onderzoek (NWO), Netherlands; The Research Council of Norway, Norway; Commission on Science and Technology for Sustainable Development in the South (COMSATS), Pakistan; Pontificia Universidad Católica del Perú, Peru; Ministry of Education and Science, National Science Centre and WUT ID-UB, Poland; Korea Institute of Science and Technology Information and National Research Foundation of Korea (NRF), Republic of Korea; Ministry of Education and Scientific Research, Institute of Atomic Physics, Ministry of Research and Innovation and Institute of Atomic Physics and Universitatea Nationala de Stiinta si Tehnologie Politehnica Bucuresti, Romania; Ministry of Education, Science, Research and Sport of the Slovak Republic, Slovakia; National Research Foundation of South Africa, South Africa; Swedish Research Council (VR) and Knut & Alice Wallenberg Foundation (KAW), Sweden; European Organization for Nuclear Research, Switzerland; Suranaree University of Technology (SUT), National Science and Technology Development Agency (NSTDA) and National Science, Research and Innovation Fund (NSRF via PMU-B B05F650021), Thailand; Turkish Energy, Nuclear and Mineral Research Agency (TENMAK), Turkey; National Academy of Sciences of Ukraine, Ukraine; Science and Technology Facilities Council (STFC), United Kingdom; National Science Foundation of the United States of America (NSF) and United States Department of Energy, Office of Nuclear Physics (DOE NP), United States of America. In addition, individual groups or members have received support from: Czech Science Foundation (grant no. 23-07499S), Czech Republic; European Research Council, Strong 2020 - Horizon 2020 (grant nos. 950692, 824093), European Union; ICSC - Centro Nazionale di Ricerca in High Performance Computing, Big Data and Quantum Computing, European Union - NextGenerationEU; Academy of Finland (Center of Excellence in Quark Matter) (grant nos. 346327, 346328), Finland.

References

- [1] H. H. Gutbrod *et al.*, “Final-state interactions in the production of hydrogen and helium isotopes by relativistic heavy ions on uranium”, *Phys. Rev. Lett.* **37** (1976) 667–670.

- [2] J. Gosset *et al.*, “Central Collisions of Relativistic Heavy Ions”, *Phys. Rev. C* **16** (1977) 629–657.
- [3] S. Nagamiya *et al.*, “Production of pions and light fragments at large angles in high-energy nuclear collisions”, *Phys. Rev. C* **24** (1981) 971–1009.
- [4] S. Nagamiya, J. Randrup, and T. J. M. Symons, “Nuclear collisions at high-energies”, *Ann. Rev. Nucl. Part. Sci.* **34** (1984) 155–187.
- [5] R. L. Auble *et al.*, “Light ion emission from reactions induced by 0.8-2.4 GeV ^{16}O projectiles”, *Phys. Rev. C* **28** (1983) 1552–1564.
- [6] **E886** Collaboration, N. Saito *et al.*, “Composite particle production in relativistic Au+Pt, Si+Pt, and p+Pt collisions”, *Phys. Rev. C* **49** (1994) 3211–3218.
- [7] T. Abbott *et al.*, “Charged hadron distributions in central and peripheral Si + A collisions at 14.6A GeV/c”, *Phys. Rev. C* **50** (1994) 1024–1047.
- [8] **E814** Collaboration, J. Barrette *et al.*, “Production of light nuclei in relativistic heavy-ion collisions”, *Phys. Rev. C* **50** (1994) 1077–1084.
- [9] **EOS** Collaboration, S. Wang *et al.*, “Light fragment production and power law behavior in Au + Au collisions”, *Phys. Rev. Lett.* **74** (1995) 2646–2649.
- [10] **NA44** Collaboration, I. G. Bearden *et al.*, “Deuteron and triton production in Pb + Pb collisions at 158 AGeV”, *Nucl. Phys. A* **661** (1999) 387–390.
- [11] **E864** Collaboration, T. A. Armstrong *et al.*, “Measurements of light nuclei production in 11.5A GeV/c Au+Pb heavy-ion collisions”, *Phys. Rev. C* **61** (2000) 064908, arXiv:nuc1-ex/0003009 [nuc1-ex].
- [12] **NA49** Collaboration, S. Afanasiev *et al.*, “Deuteron production in central Pb + Pb collisions at 158AGeV”, *Physics Letters B* **486** (2000) 22–28.
- [13] S. Albergo *et al.*, “Light nuclei production in heavy-ion collisions at relativistic energies”, *Phys. Rev. C* **65** (2002) 034907.
- [14] **NA49** Collaboration, T. Anticic *et al.*, “Energy and centrality dependence of deuteron and proton production in Pb+Pb collisions at relativistic energies”, *Phys. Rev. C* **69** (2004) 024902.
- [15] **FOPI** Collaboration, W. Reisdorf *et al.*, “Systematics of central heavy ion collisions in the 1A GeV regime”, *Nucl. Phys. A* **848** (2010) 366–427, arXiv:1005.3418 [nuc1-ex].
- [16] **NA49** Collaboration, T. Anticic *et al.*, “Production of deuterium, tritium, and ^3He in central Pb + Pb collisions at 20, 30, 40, 80, and 158 AGeV at the CERN Super Proton Synchrotron”, *Phys. Rev. C* **94** (2016) 044906.
- [17] **HADES** Collaboration, J. Adamczewski-Musch *et al.*, “Directed, Elliptic, and Higher Order Flow Harmonics of Protons, Deuterons, and Tritons in Au+Au Collisions at $\sqrt{s_{NN}} = 2.4$ GeV”, *Phys. Rev. Lett.* **125** (2020) 262301, arXiv:2005.12217 [nuc1-ex].
- [18] **STAR** Collaboration, J. Adam *et al.*, “Beam-energy dependence of the directed flow of deuterons in Au+Au collisions”, *Phys. Rev. C* **102** (2020) 044906, arXiv:2007.04609 [nuc1-ex].
- [19] **STAR** Collaboration, M. Abdallah *et al.*, “Light nuclei collectivity from $\sqrt{s_{NN}} = 3$ GeV Au+Au collisions at RHIC”, *Phys. Lett. B* **827** (2022) 136941, arXiv:2112.04066 [nuc1-ex].

- [20] **STAR** Collaboration, M. Abdulhamid *et al.*, “Beam Energy Dependence of Triton Production and Yield Ratio ($N_t \times N_p / N_d^2$) in Au+Au Collisions at RHIC”, *Phys. Rev. Lett.* **130** (2023) 202301, arXiv:2209.08058 [nucl-ex].
- [21] **STAR** Collaboration, “Production of Protons and Light Nuclei in Au+Au Collisions at $\sqrt{s_{NN}} = 3$ GeV with the STAR Detector”, arXiv:2311.11020 [nucl-ex].
- [22] **NA44** Collaboration, J. Simon-Gillo *et al.*, “Deuteron and anti-deuteron production in CERN experiment NA44”, *Nucl. Phys. A* **590** (1995) 483–486.
- [23] **NA44** Collaboration, I. G. Bearden *et al.*, “Anti-deuteron and kaon production in Pb + Pb collisions”, *Nucl. Phys.* **A661** (1999) 55–64.
- [24] **E864** Collaboration, T. A. Armstrong *et al.*, “Antideuteron Yield at the AGS and Coalescence Implications”, *Phys. Rev. Lett.* **85** (2000) 2685–2688, arXiv:nucl-ex/0005001 [nucl-ex].
- [25] M. Aoki *et al.*, “Measurements at 0° of negatively charged particles and antinuclei produced in collisions of 14.6 AGeV/c Si on Al, Cu, and Au targets”, *Phys. Rev. Lett.* **69** (1992) 2345–2348.
- [26] **NA49** Collaboration, T. Anticic *et al.*, “Antideuteron and deuteron production in midcentral Pb+Pb collisions at 158 AGeV”, *Phys. Rev. C* **85** (2012) 044913.
- [27] **NA52 (NEWMASS)** Collaboration, G. Appelquist *et al.*, “Anti-nuclei production in Pb + Pb collisions at 158 AGeV/c”, *Phys. Lett. B* **376** (1996) 245–250.
- [28] **NA52** Collaboration, M. Weber *et al.*, “The NA52 strangelet and particle search in Pb + Pb collisions at 158 AGeV/c”, *J. Phys. G* **28** (2002) 1921–1927.
- [29] **NA52** Collaboration, G. Ambrosini *et al.*, “Antimatter and matter production in heavy ion collisions at CERN: The NEWMASS experiment NA52”, *Acta Phys. Hung. A* **14** (2001) 297–308, arXiv:nucl-ex/0011016 [nucl-ex].
- [30] **NA52** Collaboration, R. Arsenescu *et al.*, “Anti-helium 3 production in lead-lead collisions at 158 AGeV”, *New J. Phys.* **5** (2003) 1.
- [31] **NA52** Collaboration, R. Arsenescu *et al.*, “An investigation of the antinuclei and nuclei production mechanism in Pb + Pb collisions at 158 AGeV”, *New J. Phys.* **5** (2003) 150.
- [32] **STAR** Collaboration, C. Adler *et al.*, “Antideuteron and anti-helium-3 production in $\sqrt{s_{NN}} = 130$ GeV Au + Au collisions”, *Phys. Rev. Lett.* **87** (2001) 262301, arXiv:nucl-ex/0108022.
- [33] **PHENIX** Collaboration, S. Afanasiev *et al.*, “Elliptic flow for phi mesons and (anti)deuterons in Au + Au collisions at $\sqrt{s_{NN}} = 200$ GeV”, *Phys. Rev. Lett.* **99** (2007) 052301, arXiv:nucl-ex/0703024 [NUCL-EX].
- [34] **PHENIX** Collaboration, S. S. Adler *et al.*, “Deuteron and Antideuteron Production in Au+Au Collisions at $\sqrt{s_{NN}} = 200$ GeV”, *Phys. Rev. Lett.* **94** (2005) 122302, arXiv:nucl-ex/0406004 [nucl-ex].
- [35] **BRAHMS** Collaboration, C. Nygaard, “Rapidity dependence of coalescence in Au+Au collisions at $\sqrt{s_{NN}} = 200$ GeV”, *J. Phys. G* **34** (2007) S1065–S1068.
- [36] **STAR** Collaboration, B. Abelev *et al.*, “Yields and elliptic flow of d(anti-d) and He-3(anti-He-3) in Au + Au collisions at $\sqrt{s_{NN}} = 200$ GeV”, arXiv:0909.0566 [nucl-ex].

- [37] **BRAHMS** Collaboration, I. Arsene *et al.*, “Rapidity dependence of deuteron production in Au+Au collisions at $\sqrt{s_{NN}} = 200$ GeV”, *Phys. Rev. C* **83** (2011) 044906, arXiv:1005.5427 [nucl-ex].
- [38] **STAR** Collaboration, J. Adam *et al.*, “Beam energy dependence of (anti-)deuteron production in Au + Au collisions at the BNL Relativistic Heavy Ion Collider”, *Phys. Rev. C* **99** (2019) 064905, arXiv:1903.11778 [nucl-ex].
- [39] **STAR** Collaboration, H. Agakishiev *et al.*, “Observation of the antimatter helium-4 nucleus”, *Nature* **473** (2011) 353, arXiv:1103.3312 [nucl-ex].
- [40] **ALICE** Collaboration, J. Adam *et al.*, “Precision measurement of the mass difference between light nuclei and anti-nuclei”, *Nature Phys.* **11** (2015) 811–814, arXiv:1508.03986 [nucl-ex].
- [41] **ALICE** Collaboration, J. Adam *et al.*, “Production of light nuclei and anti-nuclei in pp and Pb–Pb collisions at energies available at the CERN Large Hadron Collider”, *Phys. Rev. C* **93** (2016) 024917, arXiv:1506.08951 [nucl-ex].
- [42] **ALICE** Collaboration, S. Acharya *et al.*, “Production of ${}^4\text{He}$ and ${}^4\overline{\text{He}}$ in Pb–Pb collisions at $\sqrt{s_{NN}} = 2.76$ TeV at the LHC”, *Nucl. Phys. A* **971** (2018) 1–20, arXiv:1710.07531 [nucl-ex].
- [43] **ALICE** Collaboration, S. Acharya *et al.*, “Production of deuterons, tritons, ${}^3\text{He}$ nuclei and their antinuclei in pp collisions at $\sqrt{s} = 0.9, 2.76$ and 7 TeV”, *Phys. Rev. C* **97** (2018) 024615, arXiv:1709.08522 [nucl-ex].
- [44] **ALICE** Collaboration, S. Acharya *et al.*, “Multiplicity dependence of (anti-)deuteron production in pp collisions at $\sqrt{s} = 7$ TeV”, *Phys. Lett. B* **794** (2019) 50–63, arXiv:1902.09290 [nucl-ex].
- [45] **ALICE** Collaboration, S. Acharya *et al.*, “Multiplicity dependence of light (anti-)nuclei production in p–Pb collisions at $\sqrt{s_{NN}} = 5.02$ TeV”, *Phys. Lett. B* **800** (2020) 135043, arXiv:1906.03136 [nucl-ex].
- [46] **ALICE** Collaboration, S. Acharya *et al.*, “(Anti-)deuteron production in pp collisions at $\sqrt{s} = 13$ TeV”, *Eur. Phys. J. C* **80** (2020) 889, arXiv:2003.03184 [nucl-ex].
- [47] **ALICE** Collaboration, S. Acharya *et al.*, “Measurement of the low-energy antideuteron inelastic cross section”, *Phys. Rev. Lett.* **125** (2020) 162001, arXiv:2005.11122 [nucl-ex].
- [48] **ALICE** Collaboration, S. Acharya *et al.*, “Jet-associated deuteron production in pp collisions at $\sqrt{s} = 13$ TeV”, *Phys. Lett. B* **819** (2021) 136440, arXiv:2011.05898 [nucl-ex].
- [49] **ALICE** Collaboration, S. Acharya *et al.*, “Production of light (anti)nuclei in pp collisions at $\sqrt{s} = 13$ TeV”, *JHEP* **01** (2022) 106, arXiv:2109.13026 [nucl-ex].
- [50] **ALICE** Collaboration, S. Acharya *et al.*, “Production of light (anti)nuclei in pp collisions at $\sqrt{s} = 5.02$ TeV”, *Eur. Phys. J. C* **82** (2022) 289, arXiv:2112.00610 [nucl-ex].
- [51] **ALICE** Collaboration, S. Acharya *et al.*, “Measurement of anti- ${}^3\text{He}$ nuclei absorption in matter and impact on their propagation in the Galaxy”, *Nature Phys.* **19** (2023) 61–71, arXiv:2202.01549 [nucl-ex].
- [52] **ALICE** Collaboration, S. Acharya *et al.*, “First Measurement of Antideuteron Number Fluctuations at Energies Available at the Large Hadron Collider”, *Phys. Rev. Lett.* **131** (2023) 041901, arXiv:2204.10166 [nucl-ex].

- [53] **ALICE** Collaboration, S. Acharya *et al.*, “The ALICE experiment: a journey through QCD”, *Eur. Phys. J. C* **84** (2024) 813, arXiv:2211.04384 [nucl-ex].
- [54] **ALICE** Collaboration, S. Acharya *et al.*, “Light (anti)nuclei production in Pb–Pb collisions at $\sqrt{s_{NN}} = 5.02$ TeV”, *Phys. Rev. C* **107** (2023) 064904, arXiv:2211.14015 [nucl-ex].
- [55] **ALICE** Collaboration, S. Acharya *et al.*, “Enhanced Deuteron Coalescence Probability in Jets”, *Phys. Rev. Lett.* **131** (2023) 042301, arXiv:2211.15204 [nucl-ex].
- [56] **ALICE** Collaboration, S. Acharya *et al.*, “Measurement of the production of (anti)nuclei in p–Pb collisions at $s_{NN}=8.16$ TeV”, *Phys. Lett. B* **846** (2023) 137795, arXiv:2212.04777 [nucl-ex].
- [57] **ALICE** Collaboration, S. Acharya *et al.*, “Measurement of the low-energy antitriton inelastic cross section”, *Phys. Lett. B* **848** (2024) 138337, arXiv:2307.03603 [nucl-ex].
- [58] P. Braun-Munzinger and J. Stachel, “Production of strange clusters and strange matter in nucleus-nucleus collisions at the AGS”, *J. Phys. G* **21** (1995) L17–L20, arXiv:nucl-th/9412035 [nucl-th].
- [59] P. Braun-Munzinger, K. Redlich, and J. Stachel, *Particle production in heavy ion collisions, invited review in: R.C. Hwa, X.N. Wang Eds., Quark Gluon Plasma, vol. 3.* World Scientific Publishing, 2003. arXiv:nucl-th/0304013.
- [60] A. Andronic *et al.*, “Production of light nuclei, hypernuclei and their antiparticles in relativistic nuclear collisions”, *Phys. Lett. B* **697** (2011) 203–207, arXiv:1010.2995 [nucl-th].
- [61] P. Braun-Munzinger and B. Dönigus, “Loosely-bound objects produced in nuclear collisions at the LHC”, *Nucl. Phys. A* **987** (2019) 144–201, arXiv:1809.04681 [nucl-ex].
- [62] A. Andronic *et al.*, “Decoding the phase structure of QCD via particle production at high energy”, *Nature* **561** (2018) 321–330, arXiv:1710.09425 [nucl-th].
- [63] V. Vovchenko, B. Dönigus and H. Stoecker, “Multiplicity dependence of light nuclei production at LHC energies in the canonical statistical model”, *Phys. Lett. B* **785** (2018) 171–174, arXiv:1808.05245 [hep-ph].
- [64] B. Dönigus, “Light nuclei in the hadron resonance gas”, *Int. J. Mod. Phys. E* **29** (2020) 2040001, arXiv:2004.10544 [nucl-th].
- [65] **HotQCD** Collaboration, A. Bazavov *et al.*, “Chiral crossover in QCD at zero and non-zero chemical potentials”, *Phys. Lett. B* **795** (2019) 15–21, arXiv:1812.08235 [hep-lat].
- [66] S. Borsanyi, Z. Fodor, J. N. Guenther, R. Kara, S. D. Katz, P. Parotto, A. Pasztor, C. Ratti, and K. K. Szabo, “QCD Crossover at Finite Chemical Potential from Lattice Simulations”, *Phys. Rev. Lett.* **125** (2020) 052001, arXiv:2002.02821 [hep-lat].
- [67] V. Vovchenko, K. Gallmeister, J. Schaffner-Bielich, and C. Greiner, “Nucleosynthesis in heavy-ion collisions at the LHC via the Saha equation”, *Phys. Lett. B* **800** (2020) 135131, arXiv:1903.10024 [hep-ph].
- [68] V. Vovchenko and V. Koch, “Centrality dependence of proton and light nuclei yields as a consequence of baryon annihilation in the hadronic phase”, *Phys. Lett. B* **835** (2022) 137577, arXiv:2210.15641 [nucl-th].
- [69] S. Butler and C. Pearson, “Deuterons from high-energy proton bombardment of matter”, *Phys. Rev.* **129** (1963) 836–842.

- [70] J. I. Kapusta, “Mechanisms for deuteron production in relativistic nuclear collisions”, *Phys. Rev. C* **21** (1980) 1301–1310.
- [71] L. Csernai and J. I. Kapusta, “Entropy and Cluster Production in Nuclear Collisions”, *Phys. Rept.* **131** (1986) 223–318.
- [72] J. Steinheimer *et al.*, “Hypernuclei, dibaryon and antinuclei production in high energy heavy ion collisions: Thermal production versus Coalescence”, *Phys. Lett. B* **714** (2012) 85–91, arXiv:1203.2547 [nucl-th].
- [73] K.-J. Sun, R. Wang, C. M. Ko, Y.-G. Ma, and C. Shen, “Unveiling the dynamics of little-bang nucleosynthesis”, *Nature Commun.* **15** (2024) 1074, arXiv:2207.12532 [nucl-th].
- [74] T. Sjöstrand *et al.*, “An introduction to PYTHIA 8.2”, *Comput. Phys. Commun.* **191** (2015) 159–177, arXiv:1410.3012 [hep-ph].
- [75] C. Bierlich *et al.*, “A comprehensive guide to the physics and usage of PYTHIA 8.3”, arXiv:2203.11601 [hep-ph].
- [76] T. Pierog *et al.*, “EPOS LHC: Test of collective hadronization with data measured at the CERN Large Hadron Collider”, *Phys. Rev. C* **92** (2015) 034906, arXiv:1306.0121 [hep-ph].
- [77] S. Bass *et al.*, “Microscopic models for ultrarelativistic heavy ion collisions”, *Prog.Part.Nucl. Phys.* **41** (1998) 255–369, arXiv:nucl-th/9803035 [nucl-th].
- [78] S. Sombun *et al.*, “Deuteron production from phase-space coalescence in the UrQMD approach”, *Phys. Rev. C* **99** (2019) 014901, arXiv:1805.11509 [nucl-th].
- [79] T. Reichert *et al.*, “Energy dependence of light hypernuclei production in heavy-ion collisions from a coalescence and statistical-thermal model perspective”, *Phys. Rev. C* **107** (2023) 014912, arXiv:2210.11876 [nucl-th].
- [80] D. Oliinychenko, L.-G. Pang, H. Elfner, and V. Koch, “Centrality dependence of deuteron production in Pb+Pb collisions at 2.76 TeV via hydrodynamics and hadronic afterburner”, *MDPI Proc.* **10** (2019) 6, arXiv:1812.06225 [hep-ph].
- [81] D. Oliinychenko, L.-G. Pang, H. Elfner, and V. Koch, “Microscopic study of deuteron production in PbPb collisions at $\sqrt{s} = 2.76$ TeV via hydrodynamics and a hadronic afterburner”, *Phys. Rev. C* **99** (2019) 044907, arXiv:1809.03071 [hep-ph].
- [82] H. Petersen *et al.*, “SMASH – A new hadronic transport approach”, *Nucl. Phys. A* **982** (2019) 399–402, arXiv:1808.06832 [nucl-th].
- [83] S. Mrowczynski, “Deuteron formation mechanism”, *J. Phys. G* **13** (1987) 1089–1097.
- [84] S. Mrowczynski, “Anti-deuteron Production and the Size of the Interaction Zone”, *Phys. Lett. B* **248** (1990) 459–463.
- [85] S. Mrowczynski, “On the neutron proton correlations and deuteron production”, *Phys. Lett. B* **277** (1992) 43–48.
- [86] R. Scheibl and U. W. Heinz, “Coalescence and flow in ultrarelativistic heavy ion collisions”, *Phys. Rev. C* **59** (1999) 1585–1602, arXiv:nucl-th/9809092 [nucl-th].
- [87] K. Blum, R. Sato, and E. Waxman, “Cosmic-ray Antimatter”, arXiv:1709.06507 [astro-ph.HE].

- [88] K.-J. Sun and L.-W. Chen, “Analytical coalescence formula for particle production in relativistic heavy-ion collisions”, *Phys. Rev. C* **95** (2017) 044905, arXiv:1701.01935 [nucl-th].
- [89] K.-J. Sun, C.-M. Ko and B. Dönigus, “Suppression of light nuclei production in collisions of small systems at the Large Hadron Collider”, *Phys. Lett. B* **792** (2019) 132–137, arXiv:1812.05175 [nucl-th].
- [90] K. Blum and M. Takimoto, “Nuclear coalescence from correlation functions”, *Phys. Rev. C* **99** (2019) 044913, arXiv:1901.07088 [nucl-th].
- [91] F. Bellini and A. P. Kalweit, “Testing production scenarios for (anti-)(hyper-)nuclei and exotica at energies available at the CERN Large Hadron Collider”, *Phys. Rev. C* **99** (2019) 054905, arXiv:1807.05894 [hep-ph].
- [92] F. Bellini and A. P. Kalweit, “Testing production scenarios for (anti-)(hyper-)nuclei with multiplicity-dependent measurements at the LHC”, *Acta Phys. Polon. B* **50** (2019) 991, arXiv:1907.06868 [hep-ph].
- [93] F. Bellini, K. Blum, A. P. Kalweit, and M. Puccio, “Examination of coalescence as the origin of nuclei in hadronic collisions”, *Phys. Rev. C* **103** (2021) 014907, arXiv:2007.01750 [nucl-th].
- [94] F. Becattini *et al.*, “Features of particle multiplicities and strangeness production in central heavy ion collisions between 1.7 AGeV/c and 158 AGeV/c”, *Phys. Rev. C* **64** (2001) 024901, arXiv:hep-ph/0002267 [hep-ph].
- [95] N. Sharma, J. Cleymans, B. Hippolyte, and M. Paradza, “A Comparison of p-p, p–Pb, Pb–Pb Collisions in the Thermal Model: Multiplicity Dependence of Thermal Parameters”, *Phys. Rev. C* **99** (2019) 044914, arXiv:1811.00399 [hep-ph].
- [96] V. Vovchenko, B. Dönigus and H. Stoecker, “Canonical statistical model analysis of p-p, p–Pb, and Pb–Pb collisions at energies available at the CERN Large Hadron Collider”, *Phys. Rev. C* **100** (2019) 054906, arXiv:1906.03145 [hep-ph].
- [97] N. Sharma, L. Kumar, P. M. Lo, and K. Redlich, “Light-nuclei production in pp and pA collisions in the baryon canonical ensemble approach”, *Phys. Rev. C* **107** (2023) 054903, arXiv:2210.15617 [nucl-th].
- [98] E. Schnedermann, J. Sollfrank, and U. W. Heinz, “Thermal phenomenology of hadrons from 200 AGeV S+S collisions”, *Phys. Rev. C* **48** (1993) 2462–2475, arXiv:nucl-th/9307020 [nucl-th].
- [99] J. Cleymans, S. Kabana, I. Kraus, H. Oeschler, K. Redlich, *et al.*, “Antimatter production in proton-proton and heavy-ion collisions at ultrarelativistic energies”, *Phys. Rev. C* **84** (2011) 054916, arXiv:1105.3719 [hep-ph].
- [100] U. W. Heinz, P. R. Subramanian, H. Stoecker, and W. Greiner, “Formation of Antimatter Clusters in the Hadronization Phase Transition”, *J. Phys. G* **12** (1986) 1237.
- [101] W. Greiner, “Fundamental issues in the physics of elementary matter: Cold valleys and fusion of superheavy nuclei - hypernuclei - antinuclei - correlations in the vacuum”, *AIP Conf. Proc.* **597** (2001) 3.
- [102] W. Greiner, “Superheavy nuclei and beyond: hypermatter and antimatter”, *Fizika B* **12** (2003) 51–60.

- [103] W. Greiner, “Superheavy nuclei and beyond: Hypermatter and antimatter”, *J. Phys. Conf. Ser.* **337** (2012) 012002.
- [104] **ALICE** Collaboration, B. Abelev *et al.*, “Centrality determination of Pb–Pb collisions at $\sqrt{s_{NN}} = 2.76$ TeV with ALICE”, *Phys. Rev. C* **88** (2013) 044909, arXiv:1301.4361 [nucl-ex].
- [105] **ALICE** Collaboration, K. Aamodt *et al.*, “The ALICE experiment at the CERN LHC”, *JINST* **3** (2008) S08002.
- [106] **ALICE** Collaboration, B. B. Abelev *et al.*, “Performance of the ALICE Experiment at the CERN LHC”, *Int. J. Mod. Phys. A* **29** (2014) 1430044, arXiv:1402.4476 [nucl-ex].
- [107] **ALICE** Collaboration, K. Aamodt *et al.*, “Alignment of the ALICE Inner Tracking System with cosmic-ray tracks”, *JINST* **5** (2010) P03003, arXiv:1001.0502 [physics.ins-det].
- [108] J. Alme *et al.*, “The ALICE TPC, a large 3-dimensional tracking device with fast readout for ultra-high multiplicity events”, *Nucl. Instrum. Meth. A* **622** (2010) 316–367, arXiv:1001.1950 [physics.ins-det].
- [109] A. Akhondinov *et al.*, “Performance of the ALICE Time-Of-Flight detector at the LHC”, *Eur. Phys. J. Plus* **128** (2013) 44.
- [110] **ALICE** Collaboration, S. Acharya *et al.*, “The ALICE Transition Radiation Detector: construction, operation, and performance”, *Nucl. Instrum. Meth. A* **881** (2018) 88–127, arXiv:1709.02743 [physics.ins-det].
- [111] **ALICE** Collaboration, E. Abbas *et al.*, “Performance of the ALICE VZERO system”, *JINST* **8** (2013) P10016, arXiv:1306.3130 [nucl-ex].
- [112] W. Herr, “Beam-beam interactions”, <https://cds.cern.ch/record/941319>.
- [113] X.-N. Wang and M. Gyulassy, “HIJING: A Monte Carlo model for multiple jet production in pp, pA and AA collisions”, *Phys. Rev.* **D44** (1991) 3501–3516.
- [114] **GEANT4** Collaboration, S. Agostinelli *et al.*, “GEANT4: A Simulation toolkit”, *Nucl. Instrum. Meth.* **A506** (2003) 250–303.
- [115] R. Barlow, “Systematic errors: Facts and fictions”, in *Advanced Statistical Techniques in Particle Physics.*, pp. 134–144. 2002. arXiv:hep-ex/0207026 [hep-ex]. <http://www.ippp.dur.ac.uk/Workshops/02/statistics/proceedings//barlow.pdf>.
- [116] **ALICE** Collaboration, S. Acharya *et al.*, “Production of charged pions, kaons, and (anti-)protons in Pb–Pb and inelastic pp collisions at $\sqrt{s_{NN}} = 5.02$ TeV”, *Phys. Rev. C* **101** (2020) 044907, arXiv:1910.07678 [nucl-ex].
- [117] V. M. Grichine, “A simple model for integral hadron-nucleus and nucleus-nucleus cross-sections”, *Nucl. Instrum. Meth. B* **267** (2009) 2460–2462.
- [118] V. Uzhinsky *et al.*, “Antinucleus-nucleus cross sections implemented in Geant4”, *Phys. Lett. B* **705** (2011) 235–239.
- [119] J. Allison *et al.*, “Recent developments in Geant4”, *Nucl. Instrum. Meth. A* **835** (2016) 186–225.
- [120] **ALICE** Collaboration, B. Abelev *et al.*, “Centrality dependence of π , K, p production in Pb–Pb collisions at $\sqrt{s_{NN}} = 2.76$ TeV”, *Phys. Rev. C* **88** (2013) 044910, arXiv:1303.0737 [hep-ex].

- [121] A. Mazeliauskas, S. Floerchinger, E. Grossi, and D. Teaney, “Fast resonance decays in nuclear collisions”, *Eur. Phys. J. C* **79** (2019) 284, arXiv:1809.11049 [nucl-th].
- [122] A. Mazeliauskas, S. Floerchinger, E. Grossi, and D. Teaney, “FastReso–program for computing irreducible components of the particle distribution from direct resonance decays, GitHub repository”, <https://github.com/amazeliauskas/FastReso>. 2019.
- [123] A. Mazeliauskas and V. Vislavicius, “Temperature and fluid velocity on the freeze-out surface from π , K , p spectra in pp, p–Pb and Pb–Pb collisions”, *Phys. Rev. C* **101** (2020) 014910, arXiv:1907.11059 [hep-ph].
- [124] S. Grigoryan, “A three component model for hadron p_T -spectra in pp and Pb–Pb collisions at the LHC”, *Eur. Phys. J. A* **57** (2021) 328, arXiv:2109.07888 [hep-ph].
- [125] V. Vovchenko and H. Stoecker, “Thermal-FIST: A package for heavy-ion collisions and hadronic equation of state”, *Comput. Phys. Commun.* **244** (2019) 295–310, arXiv:1901.05249 [nucl-th].
- [126] ALICE Collaboration, S. Acharya *et al.*, “Production of (anti-) ^3He and (anti-) ^3H in p–Pb collisions at $\sqrt{s_{\text{NN}}} = 5.02$ TeV”, *Phys. Rev. C* **101** (2020) 044906, arXiv:1910.14401 [nucl-ex].
- [127] J. Steinheimer, calculation based on [72, 79], 2023.
- [128] K.-J. Sun, calculation based on [88, 89], 2023.
- [129] R. Wang, C. Han, and X. Chen, “Exploring the mass radius of He4 and implications for nuclear structure”, *Phys. Rev. C* **109** (2024) L012201, arXiv:2309.01416 [hep-ph].
- [130] I. Angeli and K. P. Marinova, “Table of experimental nuclear ground state charge radii: An update”, *Atom. Data Nucl. Data Tabl.* **99** (2013) 69–95.
- [131] J. J. Krauth *et al.*, “Measuring the α -particle charge radius with muonic helium-4 ions”, *Nature* **589** (2021) 527–531.

A The ALICE Collaboration

S. Acharya ¹²⁸, D. Adamová ⁸⁷, G. Aglieri Rinella ³³, M. Agnello ³⁰, N. Agrawal ⁵², Z. Ahammed ¹³⁶, S. Ahmad ¹⁶, S.U. Ahn ⁷², I. Ahuja ³⁸, A. Akhmedov ¹⁴², M. Al-Turany ⁹⁸, D. Aleksandrov ¹⁴², B. Alessandro ⁵⁷, H.M. Alfanda ⁶, R. Alfaro Molina ⁶⁸, B. Ali ¹⁶, A. Alici ²⁶, N. Alizadehvandchali ¹¹⁷, A. Alkin ³³, J. Alme ²¹, G. Alocco ⁵³, T. Alt ⁶⁵, A.R. Altamura ⁵¹, I. Altsybeev ⁹⁶, J.R. Alvarado ⁴⁵, M.N. Anaam ⁶, C. Andrei ⁴⁶, N. Andreou ¹¹⁶, A. Andronic ¹²⁷, E. Andronov ¹⁴², V. Anguelov ⁹⁵, F. Antinori ⁵⁵, P. Antonioli ⁵², N. Apadula ⁷⁵, L. Aphecetche ¹⁰⁴, H. Appelshäuser ⁶⁵, C. Arata ⁷⁴, S. Arcelli ²⁶, M. Aresti ²³, R. Arnaldi ⁵⁷, J.G.M.C.A. Arneiro ¹¹¹, I.C. Arsene ²⁰, M. Arslandok ¹³⁹, A. Augustinus ³³, R. Averbeck ⁹⁸, M.D. Azmi ¹⁶, H. Baba ¹²⁵, A. Badalà ⁵⁴, J. Bae ¹⁰⁵, Y.W. Baek ⁴¹, X. Bai ¹²¹, R. Bailhache ⁶⁵, Y. Bailung ⁴⁹, R. Bala ⁹², A. Balbino ³⁰, A. Baldisseri ¹³¹, B. Balis ², D. Banerjee ⁴, Z. Banoo ⁹², F. Barile ³², L. Barioglio ⁹⁶, M. Barlou ⁷⁹, B. Barman ⁴², G.G. Barnaföldi ⁴⁷, L.S. Barnby ⁸⁶, E. Barreau ¹⁰⁴, V. Barret ¹²⁸, L. Barreto ¹¹¹, C. Bartels ¹²⁰, K. Barth ³³, E. Bartsch ⁶⁵, N. Bastid ¹²⁸, S. Basu ⁷⁶, G. Batigne ¹⁰⁴, D. Battistini ⁹⁶, B. Batyunya ¹⁴³, D. Bauri ⁴⁸, J.L. Bazo Alba ¹⁰², I.G. Bearden ⁸⁴, C. Beattie ¹³⁹, P. Becht ⁹⁸, D. Behera ⁴⁹, I. Belikov ¹³⁰, A.D.C. Bell Hechavarria ¹²⁷, F. Bellini ²⁶, R. Bellwied ¹¹⁷, S. Belokurova ¹⁴², L.G.E. Beltran ¹¹⁰, Y.A.V. Beltran ⁴⁵, G. Bencedi ⁴⁷, S. Beole ²⁵, Y. Berdnikov ¹⁴², A. Berdnikova ⁹⁵, L. Bergmann ⁹⁵, M.G. Besoiu ⁶⁴, L. Betev ³³, P.P. Bhaduri ¹³⁶, A. Bhasin ⁹², M.A. Bhat ⁴, B. Bhattacharjee ⁴², L. Bianchi ²⁵, N. Bianchi ⁵⁰, J. Bielčik ³⁶, J. Bielčíková ⁸⁷, A.P. Bigot ¹³⁰, A. Bilandzic ⁹⁶, G. Biro ⁴⁷, S. Biswas ⁴, N. Bize ¹⁰⁴, J.T. Blair ¹⁰⁹, D. Blau ¹⁴², M.B. Blidaru ⁹⁸, N. Bluhme ³⁹, C. Blume ⁶⁵, G. Boca ^{22,56}, F. Bock ⁸⁸, T. Bodova ²¹, S. Boi ²³, J. Bok ¹⁷, L. Boldizsár ⁴⁷, M. Bombara ³⁸, P.M. Bond ³³, G. Bonomi ^{135,56}, H. Borel ¹³¹, A. Borissov ¹⁴², A.G. Borquez Carcamo ⁹⁵, H. Bossi ¹³⁹, E. Botta ²⁵, Y.E.M. Bouziani ⁶⁵, L. Bratrud ⁶⁵, P. Braun-Munzinger ⁹⁸, M. Bregant ¹¹¹, M. Broz ³⁶, G.E. Bruno ^{97,32}, M.D. Buckland ²⁴, D. Budnikov ¹⁴², H. Buesching ⁶⁵, S. Bufalino ³⁰, P. Buhler ¹⁰³, N. Burmasov ¹⁴², Z. Buthelezi ^{69,124}, A. Bylinkin ²¹, S.A. Bysiak ¹⁰⁸, J.C. Cabanillas Noris ¹¹⁰, M. Cai ⁶, H. Caines ¹³⁹, A. Caliva ²⁹, E. Calvo Villar ¹⁰², J.M.M. Camacho ¹¹⁰, P. Camerini ²⁴, F.D.M. Canedo ¹¹¹, S.L. Cantway ¹³⁹, M. Carabas ¹¹⁴, A.A. Carballo ³³, F. Carnesecchi ³³, R. Caron ¹²⁹, L.A.D. Carvalho ¹¹¹, J. Castillo Castellanos ¹³¹, F. Catalano ^{33,25}, C. Ceballos Sanchez ¹⁴³, I. Chakaberia ⁷⁵, P. Chakraborty ⁴⁸, S. Chandra ¹³⁶, S. Chapeland ³³, M. Chartier ¹²⁰, S. Chattopadhyay ¹³⁶, S. Chattopadhyay ¹⁰⁰, T. Cheng ^{98,6}, C. Cheshkov ¹²⁹, B. Cheynis ¹²⁹, V. Chibante Barroso ³³, D.D. Chinellato ¹¹², E.S. Chizzali ^{11,96}, J. Cho ⁵⁹, S. Cho ⁵⁹, P. Chochula ³³, D. Choudhury ⁴², P. Christakoglou ⁸⁵, C.H. Christensen ⁸⁴, P. Christiansen ⁷⁶, T. Chujo ¹²⁶, M. Ciaccio ³⁰, C. Cicalo ⁵³, M.R. Ciupek ⁹⁸, G. Clai ^{III,52}, F. Colamaria ⁵¹, J.S. Colburn ¹⁰¹, D. Colella ^{97,32}, M. Colocci ²⁶, M. Concas ³³, G. Conesa Balbastre ⁷⁴, Z. Conesa del Valle ¹³², G. Contin ²⁴, J.G. Contreras ³⁶, M.L. Coquet ¹³¹, P. Cortese ^{134,57}, M.R. Cosentino ¹¹³, F. Costa ³³, S. Costanza ^{22,56}, C. Cot ¹³², J. Crkovská ⁹⁵, P. Crochet ¹²⁸, R. Cruz-Torres ⁷⁵, P. Cui ⁶, A. Dainese ⁵⁵, M.C. Danisch ⁹⁵, A. Danu ⁶⁴, P. Das ⁸¹, P. Das ⁴, S. Das ⁴, A.R. Dash ¹²⁷, S. Dash ⁴⁸, A. De Caro ²⁹, G. de Cataldo ⁵¹, J. de Cuveland ³⁹, A. De Falco ²³, D. De Gruttola ²⁹, N. De Marco ⁵⁷, C. De Martin ²⁴, S. De Pasquale ²⁹, R. Deb ¹³⁵, R. Del Grande ⁹⁶, L. Dello Stritto ^{33,29}, W. Deng ⁶, P. Dhankher ¹⁹, D. Di Bari ³², A. Di Mauro ³³, B. Diab ¹³¹, R.A. Diaz ^{143,7}, T. Dietel ¹¹⁵, Y. Ding ⁶, J. Ditzel ⁶⁵, R. Divià ³³, D.U. Dixit ¹⁹, Ø. Djuvsland ²¹, U. Dmitrieva ¹⁴², A. Dobrin ⁶⁴, B. Dönigus ⁶⁵, J.M. Dubinski ¹³⁷, A. Dubla ⁹⁸, S. Dudi ⁹¹, P. Dupieux ¹²⁸, M. Durkac ¹⁰⁷, N. Dzalaiova ¹³, T.M. Eder ¹²⁷, R.J. Ehlers ⁷⁵, F. Eisenhut ⁶⁵, R. Ejima ⁹³, D. Elia ⁵¹, B. Erazmus ¹⁰⁴, F. Ercolessi ²⁶, B. Espagnon ¹³², G. Eulisse ³³, D. Evans ¹⁰¹, S. Evdokimov ¹⁴², L. Fabbietti ⁹⁶, M. Faggin ²⁸, J. Faivre ⁷⁴, F. Fan ⁶, W. Fan ⁷⁵, A. Fantoni ⁵⁰, M. Fasel ⁸⁸, A. Feliciello ⁵⁷, G. Feofilov ¹⁴², A. Fernández Téllez ⁴⁵, L. Ferrandi ¹¹¹, M.B. Ferrer ³³, A. Ferrero ¹³¹, C. Ferrero ^{IV,57}, A. Ferretti ²⁵, V.J.G. Feuillard ⁹⁵, V. Filova ³⁶, D. Finogeev ¹⁴², F.M. Fionda ⁵³, E. Flatland ³³, F. Flor ¹¹⁷, A.N. Flores ¹⁰⁹, S. Foertsch ⁶⁹, I. Fokin ⁹⁵, S. Fokin ¹⁴², E. Fragiaco ⁵⁸, E. Frajna ⁴⁷, U. Fuchs ³³, N. Funicello ²⁹, C. Furget ⁷⁴, A. Furs ¹⁴², T. Fusayasu ⁹⁹, J.J. Gaardhøje ⁸⁴, M. Gagliardi ²⁵, A.M. Gago ¹⁰², T. Gahlaut ⁴⁸, C.D. Galvan ¹¹⁰, D.R. Gangadharan ¹¹⁷, P. Ganoti ⁷⁹, C. Garabatos ⁹⁸, T. García Chávez ⁴⁵, E. Garcia-Solis ⁹, C. Gargiulo ³³, P. Gasik ⁹⁸, A. Gautam ¹¹⁹, M.B. Gay Ducati ⁶⁷, M. Germain ¹⁰⁴, A. Ghimouz ¹²⁶, C. Ghosh ¹³⁶, M. Giacalone ⁵², G. Gioachin ³⁰, P. Giubellino ^{98,57}, P. Giubilato ²⁸, A.M.C. Glaenzer ¹³¹, P. Glässel ⁹⁵, E. Glimos ¹²³, D.J.Q. Goh ⁷⁷, V. Gonzalez ¹³⁸, P. Gordeev ¹⁴², M. Gorgon ², K. Goswami ⁴⁹, S. Gotovac ³⁴, V. Grabski ⁶⁸, L.K. Graczykowski ¹³⁷, E. Grecka ⁸⁷, A. Grelli ⁶⁰, C. Grigoras ³³, V. Grigoriev ¹⁴², S. Grigoryan ^{143,1}, F. Grosa ³³, J.F. Grosse-Oetringhaus ³³, R. Grosso ⁹⁸, D. Grund ³⁶, N.A. Grunwald ⁹⁵, G.G. Guardiani ¹¹², R. Guernane ⁷⁴, M. Guilbaud ¹⁰⁴, K. Gulbrandsen ⁸⁴, T. Gündem ⁶⁵, T. Gunji ¹²⁵,

W. Guo ⁶, A. Gupta ⁹², R. Gupta ⁹², R. Gupta ⁴⁹, K. Gwizdziel ¹³⁷, L. Gyulai ⁴⁷, C. Hadjidakis ¹³², F.U. Haider ⁹², S. Haidlova ³⁶, M. Haldar ⁴, H. Hamagaki ⁷⁷, A. Hamdi ⁷⁵, Y. Han ¹⁴⁰, B.G. Hanley ¹³⁸, R. Hannigan ¹⁰⁹, J. Hansen ⁷⁶, J.W. Harris ¹³⁹, A. Harton ⁹, M.V. Hartung ⁶⁵, H. Hassan ¹¹⁸, D. Hatzifotiadou ⁵², P. Hauer ⁴³, L.B. Havener ¹³⁹, E. Hellbär ⁹⁸, H. Helstrup ³⁵, M. Hemmer ⁶⁵, T. Herman ³⁶, G. Herrera Corral ⁸, F. Herrmann ¹²⁷, S. Herrmann ¹²⁹, K.F. Hetland ³⁵, B. Heybeck ⁶⁵, H. Hillemanns ³³, B. Hippolyte ¹³⁰, F.W. Hoffmann ⁷¹, B. Hofman ⁶⁰, G.H. Hong ¹⁴⁰, M. Horst ⁹⁶, A. Horzyk ², Y. Hou ⁶, P. Hristov ³³, C. Hughes ¹²³, P. Huhn ⁶⁵, L.M. Huhta ¹¹⁸, T.J. Humanic ⁸⁹, A. Hutson ¹¹⁷, D. Hutter ³⁹, M.C. Hwang ¹⁹, R. Ilkaev ¹⁴², H. Ilyas ¹⁴, M. Inaba ¹²⁶, G.M. Innocenti ³³, M. Ippolitov ¹⁴², A. Isakov ^{85,87}, T. Isidori ¹¹⁹, M.S. Islam ¹⁰⁰, M. Ivanov ⁹⁸, M. Ivanov ¹³, V. Ivanov ¹⁴², K.E. Iversen ⁷⁶, M. Jablonski ², B. Jacak ^{19,75}, N. Jacazio ²⁶, P.M. Jacobs ⁷⁵, S. Jadlovská ¹⁰⁷, J. Jadlovsky ¹⁰⁷, S. Jaelani ⁸³, C. Jahnke ¹¹¹, M.J. Jakubowska ¹³⁷, M.A. Janik ¹³⁷, T. Janson ⁷¹, S. Ji ¹⁷, S. Jia ¹⁰, A.A.P. Jimenez ⁶⁶, F. Jonas ^{75,88,127}, D.M. Jones ¹²⁰, J.M. Jowett ^{33,98}, J. Jung ⁶⁵, M. Jung ⁶⁵, A. Junique ³³, A. Jusko ¹⁰¹, J. Kaewjai ¹⁰⁶, P. Kalinak ⁶¹, A.S. Kalteyer ⁹⁸, A. Kalweit ³³, A. Karasu Uysal ^{V,73}, D. Karatovic ⁹⁰, O. Karavichev ¹⁴², T. Karavicheva ¹⁴², P. Karczmarczyk ¹³⁷, E. Karpechev ¹⁴², M.J. Karwowska ^{33,137}, U. Keschull ⁷¹, R. Keidel ¹⁴¹, D.L.D. Keijdener ⁶⁰, M. Keil ³³, B. Ketzer ⁴³, S.S. Khade ⁴⁹, A.M. Khan ¹²¹, S. Khan ¹⁶, A. Khanzadeev ¹⁴², Y. Kharlov ¹⁴², A. Khatun ¹¹⁹, A. Khuntia ³⁶, Z. Khuranova ⁶⁵, B. Kileng ³⁵, B. Kim ¹⁰⁵, C. Kim ¹⁷, D.J. Kim ¹¹⁸, E.J. Kim ⁷⁰, J. Kim ¹⁴⁰, J. Kim ⁵⁹, J. Kim ⁷⁰, M. Kim ¹⁹, S. Kim ¹⁸, T. Kim ¹⁴⁰, K. Kimura ⁹³, S. Kirsch ⁶⁵, I. Kisel ³⁹, S. Kiselev ¹⁴², A. Kisiel ¹³⁷, J.P. Kitowski ², J.L. Klay ⁵, J. Klein ³³, S. Klein ⁷⁵, C. Klein-Bösing ¹²⁷, M. Kleiner ⁶⁵, T. Klemenz ⁹⁶, A. Kluge ³³, C. Kobdaj ¹⁰⁶, T. Kollegger ⁹⁸, A. Kondratyev ¹⁴³, N. Kondratyeva ¹⁴², J. Konig ⁶⁵, S.A. Konigstorfer ⁹⁶, P.J. Konopka ³³, G. Kornakov ¹³⁷, M. Korwieser ⁹⁶, S.D. Koryciak ², A. Kotliarov ⁸⁷, N. Kovacic ⁹⁰, V. Kovalenko ¹⁴², M. Kowalski ¹⁰⁸, V. Kozuharov ³⁷, I. Králik ⁶¹, A. Kravčáková ³⁸, L. Krcal ^{33,39}, M. Krivda ^{101,61}, F. Krizek ⁸⁷, K. Krizkova Gajdosova ³³, M. Kroesen ⁹⁵, M. Krüger ⁶⁵, D.M. Krupova ³⁶, E. Kryshen ¹⁴², V. Kučera ⁵⁹, C. Kuhn ¹³⁰, P.G. Kuijer ⁸⁵, T. Kumaoka ¹²⁶, D. Kumar ¹³⁶, L. Kumar ⁹¹, N. Kumar ⁹¹, S. Kumar ³², S. Kundu ³³, P. Kurashvili ⁸⁰, A. Kurepin ¹⁴², A.B. Kurepin ¹⁴², A. Kuryakin ¹⁴², S. Kushpil ⁸⁷, V. Kuskov ¹⁴², M. Kutyla ¹³⁷, M.J. Kweon ⁵⁹, Y. Kwon ¹⁴⁰, S.L. La Pointe ³⁹, P. La Rocca ²⁷, A. Lakrathok ¹⁰⁶, M. Lamanna ³³, A.R. Landou ⁷⁴, R. Langoy ¹²², P. Larionov ³³, E. Laudi ³³, L. Lautner ^{33,96}, R. Lavicka ¹⁰³, R. Lea ^{135,56}, H. Lee ¹⁰⁵, I. Legrand ⁴⁶, G. Legras ¹²⁷, J. Lehrbach ³⁹, T.M. Lelek ², R.C. Lemmon ⁸⁶, I. León Monzón ¹¹⁰, M.M. Lesch ⁹⁶, E.D. Lesser ¹⁹, P. Lévai ⁴⁷, X. Li ¹⁰, B.E. Liang-gilman ¹⁹, J. Lien ¹²², R. Lietava ¹⁰¹, I. Likmeta ¹¹⁷, B. Lim ²⁵, S.H. Lim ¹⁷, V. Lindenstruth ³⁹, A. Lindner ⁴⁶, C. Lippmann ⁹⁸, D.H. Liu ⁶, J. Liu ¹²⁰, G.S.S. Liveraro ¹¹², I.M. Lofnes ²¹, C. Loizides ⁸⁸, S. Lokos ¹⁰⁸, J. Lömker ⁶⁰, P. Loncar ³⁴, X. Lopez ¹²⁸, E. López Torres ⁷, P. Lu ^{98,121}, F.V. Lugo ⁶⁸, J.R. Luhder ¹²⁷, M. Lunardon ²⁸, G. Luparello ⁵⁸, Y.G. Ma ⁴⁰, M. Mager ³³, A. Maire ¹³⁰, E.M. Majerz ², M.V. Makariev ³⁷, M. Malaev ¹⁴², G. Malfattore ²⁶, N.M. Malik ⁹², Q.W. Malik ²⁰, S.K. Malik ⁹², L. Malinina ^{I,VIII,143}, D. Mallick ^{132,81}, N. Mallick ⁴⁹, G. Mandaglio ^{31,54}, S.K. Mandal ⁸⁰, V. Manko ¹⁴², F. Manso ¹²⁸, V. Manzari ⁵¹, Y. Mao ⁶, R.W. Marcjan ², G.V. Margagliotti ²⁴, A. Margotti ⁵², A. Marín ⁹⁸, C. Markert ¹⁰⁹, P. Martinengo ³³, M.I. Martínez ⁴⁵, G. Martínez García ¹⁰⁴, M.P.P. Martins ¹¹¹, S. Masciocchi ⁹⁸, M. Masera ²⁵, A. Masoni ⁵³, L. Massacrier ¹³², O. Massen ⁶⁰, A. Mastroserio ^{133,51}, O. Matonoha ⁷⁶, S. Mattiazzo ²⁸, A. Matyja ¹⁰⁸, C. Mayer ¹⁰⁸, A.L. Mazuecos ³³, F. Mazzaschi ²⁵, M. Mazzilli ³³, J.E. Mdhli ¹²⁴, Y. Melikyan ⁴⁴, A. Menchaca-Rocha ⁶⁸, J.E.M. Mendez ⁶⁶, E. Meninno ¹⁰³, A.S. Menon ¹¹⁷, M. Meres ¹³, Y. Miake ¹²⁶, L. Micheletti ³³, D.L. Mihaylov ⁹⁶, K. Mikhaylov ^{143,142}, D. Miśkowiec ⁹⁸, A. Modak ⁴, B. Mohanty ⁸¹, M. Mohisin Khan ^{VI,16}, M.A. Molander ⁴⁴, S. Monira ¹³⁷, C. Mordasini ¹¹⁸, D.A. Moreira De Godoy ¹²⁷, I. Morozov ¹⁴², A. Morsch ³³, T. Mrnjavac ³³, V. Muccifora ⁵⁰, S. Muhuri ¹³⁶, J.D. Mulligan ⁷⁵, A. Mulliri ²³, M.G. Munhoz ¹¹¹, R.H. Munzer ⁶⁵, H. Murakami ¹²⁵, S. Murray ¹¹⁵, L. Musa ³³, J. Musinsky ⁶¹, J.W. Myrcha ¹³⁷, B. Naik ¹²⁴, A.I. Nambrath ¹⁹, B.K. Nandi ⁴⁸, R. Nania ⁵², E. Nappi ⁵¹, A.F. Nassirpour ¹⁸, A. Nath ⁹⁵, C. Nattrass ¹²³, M.N. Naydenov ³⁷, A. Neagu ²⁰, A. Negru ¹¹⁴, E. Nekrasova ¹⁴², L. Nellen ⁶⁶, R. Nepeivoda ⁷⁶, S. Nese ²⁰, G. Neskovic ³⁹, N. Nicassio ⁵¹, B.S. Nielsen ⁸⁴, E.G. Nielsen ⁸⁴, S. Nikolaev ¹⁴², S. Nikulin ¹⁴², V. Nikulin ¹⁴², F. Noferini ⁵², S. Noh ¹², P. Nomokonov ¹⁴³, J. Norman ¹²⁰, N. Novitzky ⁸⁸, P. Nowakowski ¹³⁷, A. Nyanin ¹⁴², J. Nystrand ²¹, S. Oh ¹⁸, A. Ohlson ⁷⁶, V.A. Okorokov ¹⁴², J. Oliencz ¹³⁷, A. Onnerstad ¹¹⁸, C. Oppedisano ⁵⁷, A. Ortiz Velasquez ⁶⁶, J. Otwinowski ¹⁰⁸, M. Oya ⁹³, K. Oyama ⁷⁷, Y. Pachmayer ⁹⁵, S. Padhan ⁴⁸, D. Pagano ^{135,56}, G. Paic ⁶⁶, S. Paisano-Guzmán ⁴⁵, A. Palasciano ⁵¹, S. Panebianco ¹³¹, H. Park ¹²⁶, H. Park ¹⁰⁵, J. Park ⁵⁹, J.E. Parkkila ³³, Y. Patley ⁴⁸,

B. Paul ²³, M.M.D.M. Paulino ¹¹¹, H. Pei ⁶, T. Peitzmann ⁶⁰, X. Peng ¹¹, M. Pennisi ²⁵,
 S. Perciballi ²⁵, D. Peresunko ¹⁴², G.M. Perez ⁷, Y. Pestov ¹⁴², V. Petrov ¹⁴², M. Petrovici ⁴⁶,
 R.P. Pezzi ^{104,67}, S. Piano ⁵⁸, M. Pikna ¹³, P. Pillot ¹⁰⁴, O. Pinazza ^{52,33}, L. Pinsky ¹¹⁷, C. Pinto ⁹⁶,
 S. Pisano ⁵⁰, M. Płoskoń ⁷⁵, M. Planinic ⁹⁰, F. Pliquett ⁶⁵, M.G. Poghosyan ⁸⁸, B. Polichtchouk ¹⁴²,
 S. Politano ³⁰, N. Poljak ⁹⁰, A. Pop ⁴⁶, S. Porteboeuf-Houssais ¹²⁸, V. Pozdniakov ¹⁴³, I.Y. Pozos ⁴⁵,
 K.K. Pradhan ⁴⁹, S.K. Prasad ⁴, S. Prasad ⁴⁹, R. Preghenella ⁵², F. Prino ⁵⁷, C.A. Pruneau ¹³⁸,
 I. Pshenichnov ¹⁴², M. Puccio ³³, S. Pucillo ²⁵, Z. Pugelova ¹⁰⁷, S. Qiu ⁸⁵, L. Quaglia ²⁵, S. Ragoni ¹⁵,
 A. Rai ¹³⁹, A. Rakotozafindrabe ¹³¹, L. Ramello ^{134,57}, F. Rami ¹³⁰, T.A. Rancien ⁷⁴, M. Rasa ²⁷,
 S.S. Räsänen ⁴⁴, R. Rath ⁵², M.P. Rauch ²¹, I. Ravasenga ³³, K.F. Read ^{88,123}, C. Reckziegel ¹¹³,
 A.R. Redelbach ³⁹, K. Redlich ^{VII,80}, C.A. Reetz ⁹⁸, H.D. Regules-Medel ⁴⁵, A. Rehman ²¹, F. Reidt ³³,
 H.A. Reme-Ness ³⁵, Z. Rescakova ³⁸, K. Reygers ⁹⁵, A. Riabov ¹⁴², V. Riabov ¹⁴², R. Ricci ²⁹,
 M. Richter ²⁰, A.A. Riedel ⁹⁶, W. Riegler ³³, A.G. Riffero ²⁵, C. Ristea ⁶⁴, M.V. Rodriguez ³³,
 M. Rodríguez Cahuantzi ⁴⁵, S.A. Rodríguez Ramírez ⁴⁵, K. Røed ²⁰, R. Rogalev ¹⁴², E. Rogochaya ¹⁴³,
 T.S. Rogoschinski ⁶⁵, D. Rohr ³³, D. Röhrich ²¹, P.F. Rojas ⁴⁵, S. Rojas Torres ³⁶, P.S. Rokita ¹³⁷,
 G. Romanenko ²⁶, F. Ronchetti ⁵⁰, A. Rosano ^{31,54}, E.D. Rosas ⁶⁶, K. Roslon ¹³⁷, A. Rossi ⁵⁵,
 A. Roy ⁴⁹, S. Roy ⁴⁸, N. Rubini ²⁶, D. Ruggiano ¹³⁷, R. Rui ²⁴, P.G. Russek ², R. Russo ⁸⁵,
 A. Rustamov ⁸², E. Ryabinkin ¹⁴², Y. Ryabov ¹⁴², A. Rybicki ¹⁰⁸, H. Rytönen ¹¹⁸, J. Ryu ¹⁷,
 W. Rzesza ¹³⁷, O.A.M. Saariimaki ⁴⁴, S. Sadhu ³², S. Sadosky ¹⁴², J. Saetre ²¹, K. Šafařík ³⁶, P. Saha ⁴²,
 S.K. Saha ⁴, S. Saha ⁸¹, B. Sahoo ⁴⁸, B. Sahoo ⁴⁹, R. Sahoo ⁴⁹, S. Sahoo ⁶², D. Sahu ⁴⁹, P.K. Sahu ⁶²,
 J. Saini ¹³⁶, K. Sajdakova ³⁸, S. Sakai ¹²⁶, M.P. Salvan ⁹⁸, S. Sambyal ⁹², D. Samitz ¹⁰³, I. Sanna ^{33,96},
 T.B. Saramela ¹¹¹, D. Sarkar ⁸⁴, P. Sarma ⁴², V. Sarritzu ²³, V.M. Sarti ⁹⁶, M.H.P. Sas ³³, S. Sawan ⁸¹,
 E. Scapparone ⁵², J. Schambach ⁸⁸, H.S. Scheid ⁶⁵, C. Schiaua ⁴⁶, R. Schicker ⁹⁵, F. Schlepfer ⁹⁵,
 A. Schmah ⁹⁸, C. Schmidt ⁹⁸, H.R. Schmidt ⁹⁴, M.O. Schmidt ³³, M. Schmidt ⁹⁴, N.V. Schmidt ⁸⁸,
 A.R. Schmier ¹²³, R. Schotter ¹³⁰, A. Schröter ³⁹, J. Schukraft ³³, K. Schweda ⁹⁸, G. Scioli ²⁶,
 E. Scomparin ⁵⁷, J.E. Seger ¹⁵, Y. Sekiguchi ¹²⁵, D. Sekihata ¹²⁵, M. Selina ⁸⁵, I. Selyuzhenkov ⁹⁸,
 S. Senyukov ¹³⁰, J.J. Seo ⁹⁵, D. Serebryakov ¹⁴², L. Serkin ⁶⁶, L. Šerkšnytė ⁹⁶, A. Sevcenco ⁶⁴,
 T.J. Shaba ⁶⁹, A. Shabetai ¹⁰⁴, R. Shahoyan ³³, A. Shangaraev ¹⁴², B. Sharma ⁹², D. Sharma ⁴⁸,
 H. Sharma ⁵⁵, M. Sharma ⁹², S. Sharma ⁷⁷, S. Sharma ⁹², U. Sharma ⁹², A. Shatat ¹³², O. Sheibani ¹¹⁷,
 K. Shigaki ⁹³, M. Shimomura ⁷⁸, J. Shin ¹², S. Shirinkin ¹⁴², Q. Shou ⁴⁰, Y. Sibiriak ¹⁴², S. Siddhanta ⁵³,
 T. Siemiarczuk ⁸⁰, T.F. Silva ¹¹¹, D. Silvermyr ⁷⁶, T. Simantathammakul ¹⁰⁶, R. Simeonov ³⁷, B. Singh ⁹²,
 B. Singh ⁹⁶, K. Singh ⁴⁹, R. Singh ⁸¹, R. Singh ⁹², R. Singh ^{98,49}, S. Singh ¹⁶, V.K. Singh ¹³⁶,
 V. Singhal ¹³⁶, T. Sinha ¹⁰⁰, B. Sitar ¹³, M. Sitta ^{134,57}, T.B. Skaali ²⁰, G. Skorodumovs ⁹⁵,
 M. Slupecki ⁴⁴, N. Smirnov ¹³⁹, R.J.M. Snellings ⁶⁰, E.H. Solheim ²⁰, J. Song ¹⁷, C. Sonnabend ^{33,98},
 J.M. Sonneveld ⁸⁵, F. Soramel ²⁸, A.B. Soto-herandez ⁸⁹, R. Spijkers ⁸⁵, I. Sputowska ¹⁰⁸, J. Staa ⁷⁶,
 J. Stachel ⁹⁵, I. Stan ⁶⁴, P.J. Steffanic ¹²³, S.F. Stiefelmaier ⁹⁵, D. Stocco ¹⁰⁴, I. Storehaug ²⁰,
 P. Stratmann ¹²⁷, S. Strazzi ²⁶, A. Sturmiolo ^{31,54}, C.P. Stylianidis ⁸⁵, A.A.P. Suaide ¹¹¹, C. Suire ¹³²,
 M. Sukhanov ¹⁴², M. Suljic ³³, R. Sultanov ¹⁴², V. Sumberia ⁹², S. Sumowidagdo ⁸³, I. Szarka ¹³,
 M. Szymkowski ¹³⁷, S.F. Taghavi ⁹⁶, G. Taillepied ⁹⁸, J. Takahashi ¹¹², G.J. Tambave ⁸¹, S. Tang ⁶,
 Z. Tang ¹²¹, J.D. Tapia Takaki ¹¹⁹, N. Tapus ¹¹⁴, L.A. Tarasovicova ¹²⁷, M.G. Tazila ⁴⁶, G.F. Tassielli ³²,
 A. Tauro ³³, A. Tavira García ¹³², G. Tejeda Muñoz ⁴⁵, A. Telesca ³³, L. Terlizzi ²⁵, C. Terrevoli ¹¹⁷,
 S. Thakur ⁴, D. Thomas ¹⁰⁹, A. Tikhonov ¹⁴², N. Tiltmann ¹²⁷, A.R. Timmins ¹¹⁷, M. Tkacik ¹⁰⁷,
 T. Tkacik ¹⁰⁷, A. Toia ⁶⁵, R. Tokumoto ⁹³, K. Tomohiro ⁹³, N. Topilskaya ¹⁴², M. Toppi ⁵⁰, T. Tork ¹³²,
 V.V. Torres ¹⁰⁴, A.G. Torres Ramos ³², A. Trifiro ^{31,54}, A.S. Triolo ^{33,31,54}, S. Tripathy ⁵²,
 T. Tripathy ⁴⁸, S. Trogolo ³³, V. Trubnikov ³, W.H. Trzaska ¹¹⁸, T.P. Trzcinski ¹³⁷, A. Tumkin ¹⁴²,
 R. Turrisi ⁵⁵, T.S. Tveter ²⁰, K. Ullaland ²¹, B. Ulukutlu ⁹⁶, A. Uras ¹²⁹, M. Urioni ¹³⁵, G.L. Usai ²³,
 M. Vala ³⁸, N. Valle ²², L.V.R. van Doremalen ⁶⁰, M. van Leeuwen ⁸⁵, C.A. van Veen ⁹⁵, R.J.G. van
 Weelden ⁸⁵, P. Vande Vyvre ³³, D. Varga ⁴⁷, Z. Varga ⁴⁷, P. Vargas Torres ⁶⁶, M. Vasileiou ⁷⁹,
 A. Vasiliev ¹⁴², O. Vázquez Doce ⁵⁰, O. Vazquez Rueda ¹¹⁷, V. Vechernin ¹⁴², E. Vercellin ²⁵, S. Vergara
 Limón ⁴⁵, R. Verma ⁴⁸, L. Vermunt ⁹⁸, R. Vértesi ⁴⁷, M. Verweij ⁶⁰, L. Vickovic ³⁴, Z. Vilakazi ¹²⁴,
 O. Villalobos Baillie ¹⁰¹, A. Villani ²⁴, A. Vinogradov ¹⁴², T. Virgili ²⁹, M.M.O. Virta ¹¹⁸,
 V. Vislavicius ⁷⁶, A. Vodopyanov ¹⁴³, B. Volkel ³³, M.A. Völkl ⁹⁵, S.A. Voloshin ¹³⁸, G. Volpe ³², B. von
 Haller ³³, I. Vorobyev ³³, N. Vozniuk ¹⁴², J. Vrláková ³⁸, J. Wan ⁴⁰, C. Wang ⁴⁰, D. Wang ⁴⁰,
 Y. Wang ⁴⁰, Y. Wang ⁶, A. Wegrzynek ³³, F.T. Weiglhofer ³⁹, S.C. Wenzel ³³, J.P. Wessels ¹²⁷,
 J. Wiechula ⁶⁵, J. Wikne ²⁰, G. Wilk ⁸⁰, J. Wilkinson ⁹⁸, G.A. Willems ¹²⁷, B. Windelband ⁹⁵,
 M. Winn ¹³¹, J.R. Wright ¹⁰⁹, W. Wu ⁴⁰, Y. Wu ¹²¹, Z. Xiong ¹²¹, R. Xu ⁶, A. Yadav ⁴³, A.K. Yadav ¹³⁶,
 S. Yalcin ⁷³, Y. Yamaguchi ⁹³, S. Yang ²¹, S. Yano ⁹³, E.R. Yeats ¹⁹, Z. Yin ⁶, I.-K. Yoo ¹⁷, J.H. Yoon ⁵⁹,

H. Yu¹², S. Yuan²¹, A. Yuncu⁹⁵, V. Zaccaro²⁴, C. Zampolli³³, F. Zanone⁹⁵, N. Zardoshti³³, A. Zarochentsev¹⁴², P. Závada⁶³, N. Zaviyalov¹⁴², M. Zhalov¹⁴², B. Zhang⁶, C. Zhang¹³¹, L. Zhang⁴⁰, M. Zhang⁶, S. Zhang⁴⁰, X. Zhang⁶, Y. Zhang¹²¹, Z. Zhang⁶, M. Zhao¹⁰, V. Zhrebchevskii¹⁴², Y. Zhi¹⁰, C. Zhong⁴⁰, D. Zhou⁶, Y. Zhou⁸⁴, J. Zhu^{55,6}, Y. Zhu⁶, S.C. Zugeravel⁵⁷, N. Zurlo^{135,56}

Affiliation Notes

^I Deceased

^{II} Also at: Max-Planck-Institut für Physik, Munich, Germany

^{III} Also at: Italian National Agency for New Technologies, Energy and Sustainable Economic Development (ENEA), Bologna, Italy

^{IV} Also at: Dipartimento DET del Politecnico di Torino, Turin, Italy

^V Also at: Yildiz Technical University, Istanbul, Türkiye

^{VI} Also at: Department of Applied Physics, Aligarh Muslim University, Aligarh, India

^{VII} Also at: Institute of Theoretical Physics, University of Wrocław, Poland

^{VIII} Also at: An institution covered by a cooperation agreement with CERN

Collaboration Institutes

¹ A.I. Alikhanyan National Science Laboratory (Yerevan Physics Institute) Foundation, Yerevan, Armenia

² AGH University of Krakow, Cracow, Poland

³ Bogolyubov Institute for Theoretical Physics, National Academy of Sciences of Ukraine, Kiev, Ukraine

⁴ Bose Institute, Department of Physics and Centre for Astroparticle Physics and Space Science (CAPSS), Kolkata, India

⁵ California Polytechnic State University, San Luis Obispo, California, United States

⁶ Central China Normal University, Wuhan, China

⁷ Centro de Aplicaciones Tecnológicas y Desarrollo Nuclear (CEADEN), Havana, Cuba

⁸ Centro de Investigación y de Estudios Avanzados (CINVESTAV), Mexico City and Mérida, Mexico

⁹ Chicago State University, Chicago, Illinois, United States

¹⁰ China Institute of Atomic Energy, Beijing, China

¹¹ China University of Geosciences, Wuhan, China

¹² Chungbuk National University, Cheongju, Republic of Korea

¹³ Comenius University Bratislava, Faculty of Mathematics, Physics and Informatics, Bratislava, Slovak Republic

¹⁴ COMSATS University Islamabad, Islamabad, Pakistan

¹⁵ Creighton University, Omaha, Nebraska, United States

¹⁶ Department of Physics, Aligarh Muslim University, Aligarh, India

¹⁷ Department of Physics, Pusan National University, Pusan, Republic of Korea

¹⁸ Department of Physics, Sejong University, Seoul, Republic of Korea

¹⁹ Department of Physics, University of California, Berkeley, California, United States

²⁰ Department of Physics, University of Oslo, Oslo, Norway

²¹ Department of Physics and Technology, University of Bergen, Bergen, Norway

²² Dipartimento di Fisica, Università di Pavia, Pavia, Italy

²³ Dipartimento di Fisica dell'Università and Sezione INFN, Cagliari, Italy

²⁴ Dipartimento di Fisica dell'Università and Sezione INFN, Trieste, Italy

²⁵ Dipartimento di Fisica dell'Università and Sezione INFN, Turin, Italy

²⁶ Dipartimento di Fisica e Astronomia dell'Università and Sezione INFN, Bologna, Italy

²⁷ Dipartimento di Fisica e Astronomia dell'Università and Sezione INFN, Catania, Italy

²⁸ Dipartimento di Fisica e Astronomia dell'Università and Sezione INFN, Padova, Italy

²⁹ Dipartimento di Fisica 'E.R. Caianiello' dell'Università and Gruppo Collegato INFN, Salerno, Italy

³⁰ Dipartimento DISAT del Politecnico and Sezione INFN, Turin, Italy

³¹ Dipartimento di Scienze MIIFT, Università di Messina, Messina, Italy

³² Dipartimento Interateneo di Fisica 'M. Merlin' and Sezione INFN, Bari, Italy

³³ European Organization for Nuclear Research (CERN), Geneva, Switzerland

³⁴ Faculty of Electrical Engineering, Mechanical Engineering and Naval Architecture, University of Split, Split, Croatia

- ³⁵ Faculty of Engineering and Science, Western Norway University of Applied Sciences, Bergen, Norway
- ³⁶ Faculty of Nuclear Sciences and Physical Engineering, Czech Technical University in Prague, Prague, Czech Republic
- ³⁷ Faculty of Physics, Sofia University, Sofia, Bulgaria
- ³⁸ Faculty of Science, P.J. Šafárik University, Košice, Slovak Republic
- ³⁹ Frankfurt Institute for Advanced Studies, Johann Wolfgang Goethe-Universität Frankfurt, Frankfurt, Germany
- ⁴⁰ Fudan University, Shanghai, China
- ⁴¹ Gangneung-Wonju National University, Gangneung, Republic of Korea
- ⁴² Gauhati University, Department of Physics, Guwahati, India
- ⁴³ Helmholtz-Institut für Strahlen- und Kernphysik, Rheinische Friedrich-Wilhelms-Universität Bonn, Bonn, Germany
- ⁴⁴ Helsinki Institute of Physics (HIP), Helsinki, Finland
- ⁴⁵ High Energy Physics Group, Universidad Autónoma de Puebla, Puebla, Mexico
- ⁴⁶ Horia Hulubei National Institute of Physics and Nuclear Engineering, Bucharest, Romania
- ⁴⁷ HUN-REN Wigner Research Centre for Physics, Budapest, Hungary
- ⁴⁸ Indian Institute of Technology Bombay (IIT), Mumbai, India
- ⁴⁹ Indian Institute of Technology Indore, Indore, India
- ⁵⁰ INFN, Laboratori Nazionali di Frascati, Frascati, Italy
- ⁵¹ INFN, Sezione di Bari, Bari, Italy
- ⁵² INFN, Sezione di Bologna, Bologna, Italy
- ⁵³ INFN, Sezione di Cagliari, Cagliari, Italy
- ⁵⁴ INFN, Sezione di Catania, Catania, Italy
- ⁵⁵ INFN, Sezione di Padova, Padova, Italy
- ⁵⁶ INFN, Sezione di Pavia, Pavia, Italy
- ⁵⁷ INFN, Sezione di Torino, Turin, Italy
- ⁵⁸ INFN, Sezione di Trieste, Trieste, Italy
- ⁵⁹ Inha University, Incheon, Republic of Korea
- ⁶⁰ Institute for Gravitational and Subatomic Physics (GRASP), Utrecht University/Nikhef, Utrecht, Netherlands
- ⁶¹ Institute of Experimental Physics, Slovak Academy of Sciences, Košice, Slovak Republic
- ⁶² Institute of Physics, Homi Bhabha National Institute, Bhubaneswar, India
- ⁶³ Institute of Physics of the Czech Academy of Sciences, Prague, Czech Republic
- ⁶⁴ Institute of Space Science (ISS), Bucharest, Romania
- ⁶⁵ Institut für Kernphysik, Johann Wolfgang Goethe-Universität Frankfurt, Frankfurt, Germany
- ⁶⁶ Instituto de Ciencias Nucleares, Universidad Nacional Autónoma de México, Mexico City, Mexico
- ⁶⁷ Instituto de Física, Universidade Federal do Rio Grande do Sul (UFRGS), Porto Alegre, Brazil
- ⁶⁸ Instituto de Física, Universidad Nacional Autónoma de México, Mexico City, Mexico
- ⁶⁹ iThemba LABS, National Research Foundation, Somerset West, South Africa
- ⁷⁰ Jeonbuk National University, Jeonju, Republic of Korea
- ⁷¹ Johann-Wolfgang-Goethe Universität Frankfurt Institut für Informatik, Fachbereich Informatik und Mathematik, Frankfurt, Germany
- ⁷² Korea Institute of Science and Technology Information, Daejeon, Republic of Korea
- ⁷³ KTO Karatay University, Konya, Turkey
- ⁷⁴ Laboratoire de Physique Subatomique et de Cosmologie, Université Grenoble-Alpes, CNRS-IN2P3, Grenoble, France
- ⁷⁵ Lawrence Berkeley National Laboratory, Berkeley, California, United States
- ⁷⁶ Lund University Department of Physics, Division of Particle Physics, Lund, Sweden
- ⁷⁷ Nagasaki Institute of Applied Science, Nagasaki, Japan
- ⁷⁸ Nara Women's University (NWU), Nara, Japan
- ⁷⁹ National and Kapodistrian University of Athens, School of Science, Department of Physics, Athens, Greece
- ⁸⁰ National Centre for Nuclear Research, Warsaw, Poland
- ⁸¹ National Institute of Science Education and Research, Homi Bhabha National Institute, Jatni, India
- ⁸² National Nuclear Research Center, Baku, Azerbaijan
- ⁸³ National Research and Innovation Agency - BRIN, Jakarta, Indonesia
- ⁸⁴ Niels Bohr Institute, University of Copenhagen, Copenhagen, Denmark
- ⁸⁵ Nikhef, National institute for subatomic physics, Amsterdam, Netherlands
- ⁸⁶ Nuclear Physics Group, STFC Daresbury Laboratory, Daresbury, United Kingdom

- 87 Nuclear Physics Institute of the Czech Academy of Sciences, Husinec-Řež, Czech Republic
- 88 Oak Ridge National Laboratory, Oak Ridge, Tennessee, United States
- 89 Ohio State University, Columbus, Ohio, United States
- 90 Physics department, Faculty of science, University of Zagreb, Zagreb, Croatia
- 91 Physics Department, Panjab University, Chandigarh, India
- 92 Physics Department, University of Jammu, Jammu, India
- 93 Physics Program and International Institute for Sustainability with Knotted Chiral Meta Matter (SKCM2), Hiroshima University, Hiroshima, Japan
- 94 Physikalisches Institut, Eberhard-Karls-Universität Tübingen, Tübingen, Germany
- 95 Physikalisches Institut, Ruprecht-Karls-Universität Heidelberg, Heidelberg, Germany
- 96 Physik Department, Technische Universität München, Munich, Germany
- 97 Politecnico di Bari and Sezione INFN, Bari, Italy
- 98 Research Division and ExtreMe Matter Institute EMMI, GSI Helmholtzzentrum für Schwerionenforschung GmbH, Darmstadt, Germany
- 99 Saga University, Saga, Japan
- 100 Saha Institute of Nuclear Physics, Homi Bhabha National Institute, Kolkata, India
- 101 School of Physics and Astronomy, University of Birmingham, Birmingham, United Kingdom
- 102 Sección Física, Departamento de Ciencias, Pontificia Universidad Católica del Perú, Lima, Peru
- 103 Stefan Meyer Institut für Subatomare Physik (SMI), Vienna, Austria
- 104 SUBATECH, IMT Atlantique, Nantes Université, CNRS-IN2P3, Nantes, France
- 105 Sungkyunkwan University, Suwon City, Republic of Korea
- 106 Suranaree University of Technology, Nakhon Ratchasima, Thailand
- 107 Technical University of Košice, Košice, Slovak Republic
- 108 The Henryk Niewodniczanski Institute of Nuclear Physics, Polish Academy of Sciences, Cracow, Poland
- 109 The University of Texas at Austin, Austin, Texas, United States
- 110 Universidad Autónoma de Sinaloa, Culiacán, Mexico
- 111 Universidade de São Paulo (USP), São Paulo, Brazil
- 112 Universidade Estadual de Campinas (UNICAMP), Campinas, Brazil
- 113 Universidade Federal do ABC, Santo Andre, Brazil
- 114 Universitatea Nationala de Stiinta si Tehnologie Politehnica Bucuresti, Bucharest, Romania
- 115 University of Cape Town, Cape Town, South Africa
- 116 University of Derby, Derby, United Kingdom
- 117 University of Houston, Houston, Texas, United States
- 118 University of Jyväskylä, Jyväskylä, Finland
- 119 University of Kansas, Lawrence, Kansas, United States
- 120 University of Liverpool, Liverpool, United Kingdom
- 121 University of Science and Technology of China, Hefei, China
- 122 University of South-Eastern Norway, Kongsberg, Norway
- 123 University of Tennessee, Knoxville, Tennessee, United States
- 124 University of the Witwatersrand, Johannesburg, South Africa
- 125 University of Tokyo, Tokyo, Japan
- 126 University of Tsukuba, Tsukuba, Japan
- 127 Universität Münster, Institut für Kernphysik, Münster, Germany
- 128 Université Clermont Auvergne, CNRS/IN2P3, LPC, Clermont-Ferrand, France
- 129 Université de Lyon, CNRS/IN2P3, Institut de Physique des 2 Infinis de Lyon, Lyon, France
- 130 Université de Strasbourg, CNRS, IPHC UMR 7178, F-67000 Strasbourg, France, Strasbourg, France
- 131 Université Paris-Saclay, Centre d'Etudes de Saclay (CEA), IRFU, Département de Physique Nucléaire (DPhN), Saclay, France
- 132 Université Paris-Saclay, CNRS/IN2P3, IJCLab, Orsay, France
- 133 Università degli Studi di Foggia, Foggia, Italy
- 134 Università del Piemonte Orientale, Vercelli, Italy
- 135 Università di Brescia, Brescia, Italy
- 136 Variable Energy Cyclotron Centre, Homi Bhabha National Institute, Kolkata, India
- 137 Warsaw University of Technology, Warsaw, Poland
- 138 Wayne State University, Detroit, Michigan, United States
- 139 Yale University, New Haven, Connecticut, United States

¹⁴⁰ Yonsei University, Seoul, Republic of Korea

¹⁴¹ Zentrum für Technologie und Transfer (ZTT), Worms, Germany

¹⁴² Affiliated with an institute covered by a cooperation agreement with CERN

¹⁴³ Affiliated with an international laboratory covered by a cooperation agreement with CERN.